NASA TECHNICAL NOTE

NASA TN D-4707

NASA TN D-4707

TECH LIBRARY KAFB, NM
0131292

LOAN COPY: RETURN TO
AFWL (WLIL-2)
KIRTLAND AFB, N MEX

A THEORETICAL AND EXPERIMENTAL INVESTIGATION OF THE THREE-DIMENSIONAL VIBRATION CHARACTERISTICS OF A SCALED MODEL OF AN ASYMMETRICAL LAUNCH VEHICLE

by Ellwood L. Peele, William M. Thompson, Jr., and Christine G. Pusey

Langley Research Center
Langley Station, Hampton, Va.

RECEIVED
30 AUG 1968

NATIONAL AERONAUTICS AND SPACE ADMINISTRATION • WASHINGTON, D. C. • AUGUST 1968

TECH LIBRARY KAFB, NM
0131292

NASA TN D-4707

A THEORETICAL AND EXPERIMENTAL INVESTIGATION OF THE THREE-DIMENSIONAL VIBRATION CHARACTERISTICS OF A SCALED MODEL OF AN ASYMMETRICAL LAUNCH VEHICLE

By Ellwood L. Peele, William M. Thompson, Jr.,
and Christine G. Pusey

Langley Research Center
Langley Station, Hampton, Va.

NATIONAL AERONAUTICS AND SPACE ADMINISTRATION

For sale by the Clearinghouse for Federal Scientific and Technical Information
Springfield, Virginia 22151 – CFSTI price $3.00

A THEORETICAL AND EXPERIMENTAL INVESTIGATION OF THE THREE-DIMENSIONAL VIBRATION CHARACTERISTICS OF A SCALED MODEL OF AN ASYMMETRICAL LAUNCH VEHICLE

By Ellwood L. Peele, William M. Thompson, Jr.,
and Christine G. Pusey
Langley Research Center

SUMMARY

The three-dimensional vibration characteristics of a dynamically scaled model of an asymmetrically clustered launch vehicle were investigated both analytically and experimentally. The matrix Holzer analysis formulated specifically for this model configuration is identified as being three-dimensional because it renders possible the analysis of motion which is coupled in three planes: lateral bending motion in two planes (pitch and yaw), torsional motion, and longitudinal motion. Previous two-dimensional analyses of similar configurations considered pitch-torsion uncoupled from yaw-longitudinal motion.

The suitability of the analysis is evaluated by comparison of computed vibration characteristics with measured response of a near-replica scaled model to lateral excitation. On the basis of these comparisons, the procedure was found to be capable of predicting the major vibration characteristics. Additional comparison is made between computed data based on a coupled and uncoupled mathematical model. These comparisons indicate that for this configuration, the coupled and uncoupled analysis yielded essentially the same results.

The study also demonstrates the value of using experimental data in conjunction with analytical results to obtain a keener insight into subtle structural behavior, and thus make a contribution to improved mathematical modeling.

INTRODUCTION

An understanding of the dynamic characteristics of launch vehicles is essential to insure reliable structural designs. Ideally, design data for complex launch vehicles should be based on the results of analytical computations; however, state-of-the-art methods are not always comprehensive or reliable enough to be the sole means of predicting vehicle dynamic-response characteristics. Therefore, analytical methods for predicting the vibration response characteristics of structurally complex vehicles are

usually verified by comparison with experimental data obtained from full-scale or dynamically scaled models. Several programs have been conducted with near-replica scaled models of complex launch vehicles at the Langley Research Center. These programs include studies with models of launch-vehicle configurations consisting of: propellant tanks symmetrically clustered around a multistage center tank (refs. 1 to 3), a tandem distribution of liquid propellant tanks in a single body (ref. 4), and propellant tanks asymmetrically clustered around a center body (ref. 5). These studies have provided experimental data which enabled verification of analytical techniques adapted to these configurations.

The model configuration considered in this report represents a three-body asymmetrically oriented cluster. A matrix Holzer method has been formulated, in reference 6, for the calculation of the free vibration modes of multibodied launch vehicles both of the symmetrical and asymmetrical cluster configurations. Verification of the method was shown in reference 6 for the symmetric case through comparisons between calculated and measured vibration characteristics for the Saturn I model discussed in references 1 to 3. Similar comparisons for the asymmetric case, not given in reference 6, are given in this report. The purposes of the present report are (1) to demonstrate the applicability of the matrix Holzer fully coupled analysis to asymmetric clusters by comparisons between computed and experimentally determined modal data, (2) to compare theoretical computations for both uncoupled and coupled analyses, and (3) to illustrate the use of experimental data both to improve the mathematical models employed in the analysis and to provide more accurate numerical input data.

The experimental results were obtained during a ground vibration survey of a scaled dynamic model of the three-body clustered launch vehicle. For completeness, a brief review of the experimental phase of the test program together with a limited description of the model structure is presented in this report. Test results were obtained during lateral excitation of the model (pitch and yaw planes) when mounted in a suspension system designed to simulate free-flight boundary conditions. Data were obtained for different propellant loading conditions simulating flight times which ranged from lift-off to solid-rocket-motor burnout and for three payload masses.

SYMBOLS

F	longitudinal force
f	frequency (unmodified outrigger flexibility)
f^*	frequency (modified outrigger flexibility)

g	acceleration due to gravity; structural damping
$\bar{I}$	area moment of inertia
I	mass moment of inertia
L	any dimensional length
ℓ	maximum model length, 257.6 in. (6.54 meters)
M	yaw bending moment
M'	pitch bending moment
M_{ij}	element of generalized mass matrix
m	mass
T	torque
t	time
V	yaw shear force
V'	pitch shear force
Y	combined yaw-bending and shear deformation
Y'	combined pitch-bending and shear deformation
x,y,z	rectangular coordinates
θ	torsional angle of twist
η	scale factor
λ	frequency parameter, ω^2/g
ξ	longitudinal displacement

φ slope of yaw-bending curve

φ' slope of pitch-bending curve

ω circular frequency, $2\pi f$

Subscripts:

C beam component for center section

c computed

e experimental

f full scale

i = 1,2,3, . . . increment mass points of major beam components

m model

n number of lumped mass elements comprising beam component

N beam component for nose section

q discrete station along model span

SRM1,SRM2 solid rocket motors 1 and 2, respectively

T beam component for tail section

u uncoupled

I,II,III, . . . major internal boundaries

Superscript:

T transpose of a matrix

Matrices:

$\{\ \}$	column matrix
$[\ ]$	square or rectangular
$[P], [Q]$	transfer matrices defined in reference 6
$[U(\lambda)]$	transfer matrix for entire model
$[\overline{U}(\lambda)]$	submatrix of $[U(\lambda)]$
$\{Z\}_i$	state vector at ith station
$\{\tilde{Z}\}$	state vector of intermediate unknowns
$\{\overline{Z}\}$	state vector with homogeneous boundary conditions imposed
$[\epsilon]_i$	transfer matrix for ith elastic massless rod
$[m]_i$	transfer matrix for lumped mass
$[\sigma]$	transfer matrix for mass and elastic rod combined
$[\tilde{\sigma}]_N$	submatrix $[\sigma]_N$ compatible with $\{\overline{Z}\}$
$[\sigma]_{cluster}$	transfer matrix for SRM1, center core, SRM2 cluster

ANALYSIS

The analysis used to compute the model vibration characteristics is an application of the matrix Holzer or transfer-matrix method developed in reference 6. The matrix Holzer analysis, in review, is a matrix formulation of the tabular Holzer procedure which yields a solution, in stepwise manner, of the space-dependent part of a separable partial differential equation. The time-dependent solution is assumed sinusoidal. A set of frequencies are found, by trial and error, which give rise to inertial loadings that satisfy the external boundary conditions. This approach, also known as the transfer-matrix method, is discussed fully in reference 7. In reference 6, the procedure usually employed for single-beam configurations has been extended to provide the capability to accommodate

three-dimensional space-frame configurations. A complete derivation of the governing equations is presented in reference 6; therefore, only a brief outline of the analytical technique and its present application is given in this section.

Model Configuration

The subject of this investigation is a three-body configuration, shown in figures 1 and 2, which consists of a center core containing simulated liquid propellants and two strap-on simulated solid-propellant rocket motors oriented diametrically opposite to one another at the aft end of the core. The plane of the core and solid-rocket motor center lines is defined as the yaw plane. The pitch plane is perpendicular to the yaw plane.

The core consists of a cylindrically stiffened shell structure with fluid and mass elements distributed throughout its length. Basic components of the core are indicated in figures 1 and 2. The number of payloads and complexity of the stage III section requires additional comment. Two types of simulated payloads were employed: (1) the 26 000 lbm (11 790 kg) and 45 000 lbm (20 410 kg) simulations which consist of a thick cylindrical shell bolted to the top of the core and (2) the 5000 lbm (2268 kg) payload (fig. 2) which consists of a rigid tubular shaft flexibly mounted on the top of the core. The stage III section is considered complex since mass eccentricities are introduced by the masses used to simulate propellants and tanks which are not oriented in a radially symmetric manner.

The solid rocket motors (SRM) consist of relatively rigid steel cylinders which are attached by outriggers to the center core at the forward and aft ends as indicated in figure 2. The forward outriggers are simple tie rods designed to transmit axial loads only. Therefore, pitch and yaw bending moments and longitudinal forces are not transmitted between the core and the solid rocket motors. The aft outriggers consist of trusses which are rigidly attached to the solid rocket motor aft sections. The core-truss attachment is made through two ball joints on each side. These joints are assumed to be capable of transmitting all forces and moments with the exception of yaw bending moments. A thrust-vector control tank, containing simulated fuel, is attached to each of the solid rocket motors as indicated in figures 1 and 2.

Mathematical Model

The space-frame mathematical model, shown schematically in figure 3, consists of the following beam components: nose section, center core, solid rocket motor 1, solid rocket motor 2, and the tail section interconnected by the forward and aft outriggers. Each component is free to bend in the pitch and yaw planes, to twist, and to undergo axial deformation subject to appropriate boundary conditions. The beams representing cylindrical shell portions of the model are assumed to behave as massless rods having the

cross-sectional stiffness properties of the shell structure. The actual mass of the physical model structure is assumed to be concentrated at discrete points along each beam span and thus further subdivides the beam into elastic rod elements. The effect of mass eccentricity, which occurs when the center of gravity of a section is noncoincident with its centroid, is included. This condition exists in the model stage III because of the propellant-tank orientation and at the lower end of the solid rocket motors because of the thrust vector control tanks (TVC). (See fig. 2.) The thrust vector control tanks were assumed to be rigidly attached to the solid rocket motors and the mass was combined with the solid rocket motor mass. The addition of the mass eccentricity leads to coupling between pitch-torsion and yaw-longitudinal motion provided that the product-of-inertia terms between pitch and yaw are nonzero. The matrix Holzer analysis utilized herein is formulated to account for this fully coupled motion of the clustered configuration; this analysis is used to obtain the coupled response. However, the analysis may also be used to compute pitch-torsional motions separately from yaw-longitudinal motions and the results from this analysis are designated uncoupled responses.

Liquid masses were assumed to be rigidly attached to the beam center line in the manner of structural masses. Fluid dynamics were assumed to be negligible. Rotatory and torsional moments of inertia of the liquids were assumed to be zero.

Outline of Analytical Procedure

The analytical development is basically a problem of obtaining a matrix relationship between the load and displacement quantities at some exterior boundary to those at another, that is, the transfer matrix. These variables, also described at interior points, consist of loads and displacements for pitch, yaw, torsion, and longitudinal motion. Since each mass point is assumed to be unrestrained to ground, it will have six degrees of freedom and six corresponding loads. These quantities, given in vector form, are defined as the state vector (ref. 7) as follows:

$$\{Z\} \equiv \{V,\ M,\ \phi,\ Y \,\vdots\, V',\ M',\ \phi',\ Y' \,\vdots\, F,\ \xi \,\vdots\, T,\ \theta\}^T$$

in which:

V	shear force
M	bending moment
ϕ	bending slope
Y	displacement

F	longitudinal force
ξ	longitudinal displacement
T	axial torque
θ	angle of twist

Pitch and yaw directions are indicated by primed and unprimed symbols, respectively. The sign conventions established for these variables, when referred to any section of the model considered as a free body, are shown in figure 3(c).

The exterior stations chosen for this analysis are the nose, station I, and the aft engine, station X. The transfer between these stations is accomplished by first determining the state-vector transfer across elemental lumped-mass—weightless-rod line structures. The procedure, discussed in reference 6, is briefly as follows: the state vector $\{Z\}_{i+1}$ is related to $\{Z\}_i$ through the transfer matrix $[\sigma]$ or

$$\{Z\}_{i+1} = [\sigma]_i \{Z\}_i \tag{1}$$

where

$$[\sigma]_i = [\epsilon]_i [m]_i$$

The matrices $[\epsilon]_i$ and $[m]_i$ are transfer matrices for the individual ith massless rod and concentrated mass, respectively. The matrices used in this paper are extensions of those presented in reference 6 and are developed to satisfy the need for a more detailed description of the stiffness distribution and the inclusion of open-ended branch beams. The matrices related to the beam elements are given in detail in the appendix. Once the transfer matrices, $[\epsilon]_i$ and $[m]_i$, for the rod-mass elements are obtained, the following relationships can be established for each beam component:

$$\{Z\}_{(II,VI_C,VI_1,VI_2,X)} = [\sigma]_{(N,C,SRM1,SRM2,T)} \{Z\}_{(I,V_C,V_1,V_2,IX)} \tag{2a}$$

For example, the transfer across the nose section is given by

$$\{Z\}_{II} = [\sigma]_N \{Z\}_I \tag{2b}$$

in which

$$[\sigma]_N = [\epsilon]_n [m]_n [\epsilon]_{n-1} [m]_{n-1} \cdots [\epsilon]_i [m]_i \cdots [\epsilon]_1 [m]_1 \tag{2c}$$

In equation (2c), n denotes the number of lumped mass elements comprising the nose section.

The transfer from station II across the entire three-beam cluster to station IX is then expressed by

$$\{Z\}_{IX} = [\sigma]_{SRM1+SRM2+C+outrigger}\{Z\}_{II} = [\sigma]_{cluster}\{Z\}_{II} \tag{3}$$

The derivation of the transfer matrix $[\sigma]_{cluster}$ is very involved and is not presented here. Details of the derivation are given in reference 6. In the derivation, the internal boundary conditions of continuity and equilibrium at the forward and aft outriggers are used to obtain solutions for certain intermediate unknowns at the solid rocket forward ends. The vector consisting of the intermediate unknowns is defined as

$$\{\tilde{Z}\}_{V_k} \equiv \{V,\ V',\ T_1 \,|\, V,\ V',\ T_2 \,|\, \phi,\ \phi',\ \xi_1 \,|\, \phi,\ \phi',\ \xi_2\}^T_{V_k} \qquad (k = 1, 2)$$

Solutions for $\{\tilde{Z}\}_{V_k}$ in terms of the state vector at station I are obtained from the relation

$$\{\tilde{Z}\}_{V_k} = [Q]^{-1}[P]\{Z\}_I \tag{4}$$

in which $[Q]^{-1}$ and $[P]$ are given in reference 6. Flexibility relationships for the forward outrigger and aft truss involved in the derivation of the $[P]$ and $[Q]$ matrices are shown in the appendix. The intermediate unknowns are dependent upon the frequency parameter $\lambda = \frac{\omega^2}{g}$ assumed for the time-dependent motion and therefore must be determined for each trial frequency.

When the transfer relationship across the three-beam cluster, together with the nose and tail sections, is available, the entire model is spanned by multiplying all transfer matrices together to obtain

$$\{Z\}_X = [U(\lambda)]\{Z\}_I \tag{5}$$

in which $[U(\lambda)]$ represents the transfer matrix for the entire model. The remainder of the problem is the customary one of solving the set of homogeneous algebraic equations

$$\{\bar{Z}\}_X = [0] = [\bar{U}(\lambda)]\{\bar{Z}\}_I \tag{6}$$

where $[\bar{U}(\lambda)]$ is a submatrix of $[U(\lambda)]$ relating the external boundary conditions at X to those at I. The state vectors $\{\bar{Z}\}_X$ and $\{\bar{Z}\}_I$ reflect the homogeneous boundary conditions existing at these stations. The necessary and sufficient condition for a non-trivial solution for $\{\bar{Z}\}_I$ to exist is that the determinant $[\bar{U}(\lambda)] = 0$. This condition cannot be identically satisfied on digital computers but is approached numerically by trial-and-error methods to as many significant figures as is practical. In practice, the frequency parameter is varied over a wide range and a plot is made of the variation of

$[\bar{U}(\lambda)]$ with λ. Samples of these plots are shown in figure 4 for the matrix Holzer analysis considering both a coupled and uncoupled mathematical model. Note that the plot is discontinuous for certain values of λ. These values correspond to branch frequencies and frequencies for which $[Q]$ in equation (4) is singular. In either case, the transfer matrices will become infinitely large. Approximate zeros of this function are obtained along with the components of the corresponding vector $\{\bar{Z}\}_I$. Deflection shapes are then constructed from the state vector components corresponding to each mass point. These components are obtained numerically by transferring the variables $\{\bar{Z}\}_I$ across the model span; for example, the state vector at station II (fig. 3(b)) is found from

$$\{Z\}_{II} = [\bar{\sigma}]_N \{\bar{Z}\}_I \tag{7}$$

in which $[\bar{\sigma}]_N$ is a submatrix of $[\sigma]_N$ compatible with $\{\bar{Z}\}_I$. The types of modal motions anticipated for the asymmetric cluster are illustrated in figure 5.

Numerical Input

The input data used in the computations were largely obtained from the model manufacturer. The various stiffness properties of the core and solid-rocket-shell structures are shown in figure 6. These parameters were obtained analytically and no experimental verification of these data exists. The mass distribution of the structure is given in table I which includes the center-of-gravity location and inertial properties. The masses representing liquids and distributed shell structure were further segmented into smaller lumped masses. The number of lumped masses varies for each weight condition; however, an average of approximately 75 was employed for each configuration. Thus, systems of 450 degrees of freedom were analyzed.

Payload mounting flexibility.- The differences in physical structure between the light and heavy simulated payloads require a different mathematical representation of each payload. The light payload (5000 lbm (2268 kg)) was interpreted as an elastically mounted branch beam; however, the complexity of the mounting prohibited an accurate analytical determination of the flexibility. The mounting flexibility was therefore based on values which are related to experimentally determined pitch and yaw frequencies of 35.9 and 14.8 Hz, respectively. The heavier payloads (26 000 lbm (11 790 kg) and 45 000 lbm (20 410 kg)) were each considered to be simple continuations of the main structure, that is, the core of the model having stiffness and mass properties as shown, respectively, in figure 6 and table I.

Outrigger flexibilities.- Flexibility coefficients for the forward and aft outriggers were determined by the model manufacturer. These data, with indicated modifications, are presented in matrix form in table II and are defined by the equations shown in the

TABLE I.- MODEL COMPONENTS

Items	Mass		Center of gravity							Inertia					
			x			y		z		Roll		Pitch		Yaw	
	lbm	kg	x/l	in.	m	in.	m	in.	m	lb-in^2	N/m^2	lb-in^2	N/m^2	lb-in^2	N/m^2
Payloads															
Light	35.7	16.2	-0.007	-1.77	-0.045	0	0	12.00	0.305	531	1.52	2 310	6.63	2 310	6.63
Medium	206.9	93.85	-.094	-24.15	-.613	0	0	12.0	.305	27 901	80.07	42 890	123.1	42 890	123.1
Heavy	359.5	163.1	-.046	-11.81	-.300	0	0	12.0	.305	49 008	140.6	127 919	367.1	127 919	367.1
Stage III components															
Guidance truss	6.81	3.09	0.078	20.1	0.510	0.1	0.002	4.7	0.119	77	0.221	20	0.057	54	0.155
Equipment truss	5.44	2.46	.077	19.8	.503	1.1	.028	19.7	.500	57	.164	11	.032	53	.152
Fuel tank (full)	63.75	28.92	.124	32.0	.813	-6.9	-.175	12.0	.305	302	.867	3 057	8.77	3 057	8.77
Oxidizer tank (full)	124.35	56.40	.107	27.5	.699	4.6	.117	12.0	.305	859	2.47	5 749	16.50	5 749	16.50
Control module skirt	2.19	.99	.082	21.0	.533	0	0	12.0	.305	316	.907	186	.534	186	.534
Propulsion module and helium sphere	5.00	2.27	.109	28.1	.714	0	0	12.0	.305	350	1.00	246	.706	109	.313
Truss and engines	5.63	2.55	.146	37.6	.955	0	0	12.0	.305	329	.944	352	1.01	389	1.12
Stage II components															
Forward oxidizer skirt	7.36	3.34	0.178	45.9	1.17	0	0	12.0	0.305	1 050	3.01	1 194	3.43	1 194	3.43
Forward oxidizer dome	3.02	1.37	.214	55.2	1.40	.4	.010	11.7	.297	267	.766	149	.428	149	.428
Aft oxidizer dome	1.60	.73	.268	69.1	1.76	0	0	11.6	.295	121	.317	72	.207	75	.207
Aft oxidizer skirt	4.15	1.88	.264	68.0	1.73	0	0	12.0	.305	590	1.69	370	1.06	370	1.06
Forward fuel skirt	2.90	1.32	.310	79.8	2.03	0	0	12.0	.305	412	1.18	226	.649	226	.649
Forward fuel dome	3.16	1.43	.303	78.0	1.98	-.4	-.010	12.3	.312	279	.801	156	.448	156	.448
Aft fuel dome	2.86	1.30	.357	91.9	2.33	0	0	11.7	.297	230	.660	129	.370	129	.370
Aft fuel skirt	4.89	2.22	.357	91.9	2.33	0	0	12.0	.305	691	1.98	454	1.30	454	1.30
Equipment truss	3.94	1.79	.285	73.4	1.86	.4	.010	16.8	.427	17	.049	4	.011	15	.011
Engine simulation	11.44	5.19	.400	103.1	2.62	0	0	12.0	.305	134	.385	208	.597	208	.597
Pressure test lines in oxidizer tank	2.13	.97	.227	58.4	1.48	-3.4	-.086	15.0	.381	83	.238	44	.126	39	.126
Pressure test lines in fuel tank	2.13	.97	.316	81.3	2.07	-3.4	-.086	15.0	.381	83	.238	44	.126	39	.126
Instrumentation in oxidizer tank	1.00	.45	.227	58.4	1.48	-3.4	-.086	15.0	.381	39	.112	21	.060	18	.060
Instrumentation in fuel tank	.81	.37	.316	81.3	2.07	-3.4	-.086	15.0	.381	32	.092	17	.049	15	.049
Oxidizer fluid	343.7	155.90	.242	62.3	1.58	0	0	12.0	.305	0	0	18 688	53.63	18 688	53.63
Fuel fluid	192.7	87.4	.330	85.1	2.16	0	0	12.0	.305	0	0	8 608	24.70	8 608	24.70

TABLE I.- MODEL COMPONENTS – Concluded

Items	Mass		Center of gravity							Inertia					
			x			y		z		Roll		Pitch		Yaw	
	lbm	kg	x/ℓ	in.	M	in.	M	in.	M	lb-in^2	N-m^2	lb-in^2	N-m^2	lb-in^2	N-m^2
Stage I components															
Transportation section	9.40	4.26	0.421	108.4	2.75	0	0	12.0	0.305	1 369	3.93	1 310	3.76	990	2.84
Forward oxidizer skirt	2.81	1.27	.492	126.8	3.22	0	0	12.0	.305	399	1.15	213	.611	213	.611
Forward oxidizer dome	3.08	1.40	.486	125.1	3.18	0	0	12.0	.305	272	.781	152	.436	152	.436
Oxidizer tank barrel	15.56	7.06	.594	153.0	3.89	.8	.020	12.8	.325	1 614	4.63	2 640	7.58	2 640	7.58
Aft oxidizer dome	2.30	1.04	.709	182.7	4.64	0	0	12.0	.305	166	.476	92	.264	92	.264
Aft oxidizer skirt	2.47	1.12	.700	180.4	4.58	0	0	12.0	.305	349	1.00	194	.557	194	.557
Forward fuel skirt	4.06	1.84	.740	190.7	4.84	0	0	12.0	.305	550	1.58	898	2.58	898	2.58
Forward fuel dome	2.94	1.33	.746	192.1	4.88	0	0	12.0	.305	260	.746	145	.416	145	.416
Fuel tank barrel	18.90	8.57	.841	216.7	5.50	.4	.010	12.4	.315	1 711	4.91	3 389	9.73	3 388	9.73
Aft fuel cone	4.88	2.21	.945	243.5	6.18	0	0	12.0	.305	281	.806	210	.602	210	.602
Aft fuel skirt	7.31	3.32	.937	241.4	6.13	0	0	11.9	.302	995	2.86	2 889	8.29	2 889	8.29
Engines	37.73	17.11	1.000	257.6	6.54	0	0	12.0	.305	1 099	3.15	3 060	8.78	3 060	8.78
Pressure test lines in oxidizer tank	2.13	.97	.486	125.1	3.18	-3.4	-.086	15.0	.381	83	.238	44	.126	39	.112
Pressure test lines in fuel tank	2.13	.97	.746	192.1	4.88	-3.4	-.086	15.0	.381	83	.238	44	.126	39	.112
Oxidizer fluid	1321.1	599.2	.604	155.5	3.95	0	0	12.0	.305	0	0	435 200	1249	435 200	1249
Fuel fluid	689.5	312.8	.845	217.8	5.53	0	0	12.0	.305	0	0	151 680	435.3	151 680	435.3
One solid rocket motor (empty)															
Nose section	30.5	13.8	0.348	89.56	2.27	25.3	0.643	12.0	0.305	2 027	5.82	2 595	7.45	2 595	7.45
Barrel	270.4	122.7	.659	169.81	4.31	25.3	.643	12.0	.305	38 601	110.8	477 556	1370	477 556	1370
Aft skirt	53.19	24.1	.969	249.60	6.34	25.3	.643	12.0	.305	7 048	20.23	4 498	12.91	4 498	12.91
Aft cone	7.50	3.4	.958	246.90	6.27	25.3	.643	12.0	.305	594	1.70	330	.947	330	.947
Engine	58.63	26.6	1.000	257.60	6.54	25.8	.655	12.0	.305	1 975	5.67	3 183	9.13	3 183	9.13
Forward outriggers	1.16	.53	.390	100.5	2.55	13.3	.338	12.0	.305	167	.479	167	.479	22	.063
Aft outriggers	7.19	3.26	.952	245.27	6.23	13.3	.338	12.0	.305	1 034	2.97	1 034	2.97	135	.387
Thrust vector control tank	65.65	29.8	.721	185.77	4.72	18.2	.462	25.9	.658	1 103	3.17	37 560	107.8	37 560	107.8
Barrel (full)	305.69	138.7	.665	171.31	4.35	25.3	.643	12.0	.305	43 638	125.2	539 883	1549	539 883	1549
One solid rocket motor (full)															
Nose section	30.5	13.8	0.348	89.56	2.27	25.3	0.643	12.0	0.305	2 027	5.32	2 595	7.45	2 595	7.45
Barrel	305.69	138.7	.665	171.31	4.35	25.3	.643	12.0	.305	43 638	125.2	539 883	1549	539 883	1549
Aft skirt	53.19	24.1	.969	249.60	6.34	25.3	.643	12.0	.305	7 048	20.23	4 498	12.91	4 498	12.91
Aft cone	7.50	3.40	.958	246.90	6.27	25.3	.643	12.0	.305	594	1.70	330	.947	330	.947
Engine	58.63	26.6	1.000	257.60	6.54	25.8	.655	12.0	.315	1 975	5.67	3 183	9.13	3 183	9.13
Forward outriggers	1.16	.53	.390	100.5	2.55	13.3	.338	12.0	.305	167	.479	167	.479	22	.063
Aft outriggers	7.19	3.26	.952	245.27	6.23	13.3	.338	12.0	.305	1 034	2.97	1 034	2.97	135	.387
Thrust vector control tank	65.65	29.8	.721	185.77	4.72	18.2	.462	25.9		1 103	3.17	37 560	107.8	37 560	107.8
Ballast* per side															
Weight 1	330.30	149.8	0.429	110.52	2.81	25.3	0.643	12.0	0.305	24 624	70.67	12 577	36.09	12 577	36.09
*Weight 2	329.10	149.3	.468	120.52	3.06	25.3	.643	12.0	.305	24 335	70.41	12 532	35.96	12 532	35.96
Weight 3	329.70	149.5	.538	138.52	3.52	25.3	.643	12.0	.305	24 580	70.54	12 554	36.03	12 554	36.03
*Weight 4	331.40	150.3	.577	148.52	3.77	25.3	.643	12.0	.305	24 706	70.90	12 614	36.21	12 614	36.21
Weight 5	330.40	149.9	.650	167.52	4.26	25.3	.643	12.0	.305	24 632	70.69	12 581	36.11	12 581	36.11
*Weight 6	331.50	150.4	.685	176.55	4.48	25.3	.643	12.0	.305	24 714	70.92	12 623	36.23	12 623	36.23
Weight 7	330.80	150.0	.763	196.55	4.99	25.3	.643	12.0	.305	24 662	70.78	12 596	36.15	12 596	36.15
*Weight 8	329.80	149.6	.802	206.55	5.25	25.3	.643	12.0	.305	24 587	70.56	12 558	36.04	12 558	36.04
Weight 9	329.60	149.5	.879	226.55	5.75	25.3	.643	12.0	.305	24 572	70.52	12 551	36.02	12 551	36.02
*Weight 10	330.40	149.9	.918	236.55	6.01	25.3	.643	12.0	.305	24 632	70.69	12 581	36.11	12 581	36.11
**Thrust vector control propellant (1/2 full)	62.0	28.1	.894	230.41	5.85	18.2	.462	25.9	.658	-----	----	2 855	8.19	2 855	8.19
**Thrust vector control propellant (full)	123.90	56.2	.851	219.20	5.57	18.2	.462	25.9	.658	-----	----	21 249	60.98	21 249	60.98

*Omit to obtain data for one solid rocket motor (1/2 full).

**Omit to obtain data for one solid rocket motor (full).

TABLE II.- OUTRIGGER FLEXIBILITY COEFFICIENTS

[The coefficient matrices are defined by equations appearing in the appendix]

$$[A] = \begin{bmatrix} 3.6187 & 0.0777 & 0.5674 & 0.0292 \\ 0.0777 & 0.003375 & 0.0292 & 0.00155 \\ 0.5674 & 0.0292 & 3.6187 & 0.0777 \\ 0.0292 & 0.00155 & 0.0777 & 0.0034 \end{bmatrix} \times 10^{-5} \text{ in./lb} = \begin{bmatrix} 2.0663 & 0.0444 & 0.3240 & 0.0167 \\ 0.0444 & 0.001927 & 0.0167 & 0.000885 \\ 0.00324 & 0.0167 & 2.0663 & 0.0444 \\ 0.0167 & 0.000885 & 0.0444 & 0.001927 \end{bmatrix} \times 10^{-7} \text{ m/N}$$

$$[B] = \begin{bmatrix} 26.15 & 6.9 \\ 6.9 & 26.15 \end{bmatrix} \times 10^{-6} \text{ in./lb} = \begin{bmatrix} 14.93 & 3.9 \\ 3.9 & 14.93 \end{bmatrix} \times 10^{-8} \text{ m/N}$$

$$[C] = \begin{bmatrix} 2.8172 & 0.0428 & 0.01695 & 0.6537 & 0.02115 & 0 \\ 0.0428 & 0.00717^{**} & 0.00015 & 0.02115 & 0.00478^{**} & 0 \\ 0.01695 & 0.00015 & 0.040^{*} & 0 & 0 & 0 \\ 0.6537 & 0.002115 & 0 & 2.8172 & 0.0428 & 0.01695 \\ 0.02115 & 0.00478^{**} & 0 & 0.0428 & 0.00717^{**} & 0.00015 \\ 0 & 0 & 0 & 0.01695 & 0.00015 & 0.040^{*} \end{bmatrix} \times 10^{-5} \text{ in./lb} = \begin{bmatrix} 1.6086 & 0.02444 & 0.009679 & 0.3733 & 0.01208 & 0 \\ 0.0244 & 0.00409^{**} & 0.00086 & 0.01208 & 0.00273^{**} & 0 \\ 0.009679 & 0.000086 & 0.023^{*} & 0 & 0 & 0 \\ 0.3733 & 0.01208 & 0 & 1.6086 & 0.0244 & 0.009679 \\ 0.01208 & 0.00273^{**} & 0 & 0.0244 & 0.00409^{**} & 0.000086 \\ 0 & 0 & 0 & 0.009679 & 0.000086 & 0.023^{*} \end{bmatrix} \times 10^{-7} \text{ m/N}$$

$$[D] = \begin{bmatrix} 0 & 1 & 0 & 0 & 0 & 0 & 2.575 \times 10^{-6} \text{ (in./lb)} & 6.75 \times 10^{-6} \text{ (in./lb)} \\ \ell - a & 0 & 0 & 0 & 0 & 1 & 0 & 0 \\ 0 & 1 & 0 & 0 & 0 & 0 & 0.75 \times 10^{-6} \text{ (in./lb)} & 2.575 \times 10^{-6} \text{ (in./lb)} \\ -(\ell - a) & 0 & 0 & 0 & 0 & 1 & 0 & 0 \end{bmatrix} = \begin{bmatrix} 0 & 1 & 0 & 0 & 0 & 0 & 1.470 \times 10^{-8} \text{ (m/N)} & 0.43 \times 10^{-8} \text{ (m/N)} \\ \ell - a & 0 & 0 & 0 & 0 & 1 & 0 & 0 \\ 0 & 1 & 0 & 0 & 0 & 0 & 0.43 \times 10^{-8} \text{ (m/N)} & 1.470 \times 10^{-8} \text{ (m/N)} \\ -(\ell - a) & 0 & 0 & 0 & 0 & 1 & 0 & 0 \end{bmatrix}$$

$$[E] = \begin{bmatrix} 6.9 & -2.55 & 0 & 0 \\ -2.55 & 2.10 & 0 & 0 \\ 0 & 0 & 6.9 & 2.55 \\ 0 & 0 & -2.55 & 2.10 \end{bmatrix} \times 10^{-6} \text{ in./lb} = \begin{bmatrix} 3.9 & -1.46 & 0 & 0 \\ -1.46 & 1.20 & 0 & 0 \\ 0 & 0 & 3.9 & -1.46 \\ 0 & 0 & -1.46 & 1.20 \end{bmatrix} \times 10^{-8} \text{ m/N}$$

*Revised to reflect assumption of negligible pitch-bending moment restraint.

**Recomputed to be consistent with yaw-bending coefficients.

appendix. The coefficients reflect the assumptions that the forward outriggers are incapable of transmitting pitch and yaw bending moments or axial force. The aft outrigger coefficients reflect the assumptions that all forces and moments except yaw bending can be transmitted. Outrigger coefficients computed under these assumptions are identified as unmodified. During the present investigation, comparisons between computed and experimental vibration test results led to a reappraisal of the assumption that the aft outriggers could transmit pitch bending moment between the solid rocket motors and the core. The reasons for the reappraisal and the modifications in the coefficients are discussed fully in the section "Results and Discussion." Modal data utilizing both modified and unmodified outrigger coefficients were computed.

EXPERIMENTAL TEST APPARATUS AND PROCEDURE

Model-Scaling Considerations

Only a general description of the overall structure is presented in this report since a more detailed description of the model center core is available in reference 4. The materials used in the structure, primarily aluminum alloy, are the same as those used for the full-scale vehicle of which the model is an approximate structural replica. In some noncritical areas, different alloys of aluminum were substituted to facilitate fabrication. Whenever practical, geometric scaling was used in the design of the model to insure faithful reproduction of the main load paths and thus lead to true dynamic characteristics. It should be emphasized, however, that the structure is not a true replica model in that some components were represented by simple structural designs which are only dynamically similar to the prototype. An example of this type of dynamic scaling in basic structural members is the substitution of simple shapes for shell stiffeners for which the cross-sectional area and area moment of inertia were scaled. Other examples include lumped mass representations of equipment items, engines, and, in some cases, propellants. The various structural parameters of the model were scaled by the following relationships in which η is the scale factor:

Length:

$$L_m = \eta L_f$$

Area moment of inertia:

$$\bar{I}_m = \eta^4 \bar{I}_f$$

Mass:

$$m_m = \eta^3 m_f$$

Frequency:

$$\omega_m = \frac{1}{\eta} \omega_f$$

Mass moment of inertia:

$$I_m = \eta^5 I_f$$

Model Description

The center core of the model is a sectional structure approximately 23 feet (7 m) in length consisting of a payload, stage III section, stage II, and stage I as major components. (See fig. 1.)

The stage III section indicated in figure 1 is a relatively compact and massive component of the core in which such elements as engines and liquid propellant tanks were simulated by cylindrical steel weights. These masses were mounted on trusses in the stage III section so that the rigid-body dynamic properties simulated this part of the prototype.

The stage II section consists of the fuel tank, oxidizer tank, tank skirts, and the propulsion system. The propellant-tank skirts are basically thin-skinned (0.009 inch (0.299 mm)) shells reinforced by longitudinal and circumferential stiffeners riveted to the skin. The oxidizer tank and the fuel tank were liquid loaded and pressurized during the vibration tests. The full-scale liquid propellants were simulated in the model by liquids having the same density as the actual propellants. The various densities are shown in table III. The single-engine propulsion system for stage II was simulated by a steel cylinder.

TABLE III.- SIMULATED LIQUID PROPELLANTS

Propellant	Mixture (by weight)	Specific gravity
Oxidizer	50.2 Freon; 49.8 methylene chloride	1.42
Fuel	57.0 alcohol; 43.0 water	.93

The transportation section (which acts as the interstage between stages I and II), the two large liquid propellant tanks, and the twin-engine propulsion module constitute the first stage of the launch vehicle. The transportation section is a thin-skinned (0.009 inch (0.229 mm)) longitudinally and circumferentially stiffened structure similar in construction to the stage II tank skirts. The oxidizer and fuel tanks are also capable of pressurization and liquid loading with the same fluids (identified in table III). The propellant tanks in this stage are internally stiffened by longerons welded to the tank wall and circumferential ring stiffeners welded to the longerons.

The two identical solid rocket motors and the attached thrust vector control (TVC) fuel tanks compose the "zero stage" of the three-body configuration. Each solid motor case consists of two sectional steel barrels, a nose cone, and an aft skirt. The top and bottom of each solid rocket motor is attached to the center core by forward and aft outriggers, respectively, as indicated in figure 2. The zero-stage solid fuel was simulated by lead disks (each disk had a nominal mass of 330 lbm (149.7 kg)) evenly distributed

throughout the length of the barrel section and attached in order not to affect stiffness. Three loading conditions of the solids – empty, one-half full, and full – were simulated by installing 0, 5, or 10 lead disks, respectively. Each of the associated thrust vector control (TVC) tanks consists of two attached cylindrical sections (see fig. 1) which were designed to be fluid loaded but not pressurized.

A detailed listing of the mass and center-of-gravity location (normalized at station 257.6 in. (6.54 m)) of items comprising the major components of the model described is given in table I. The mass data for the model shown in table I were calculated by use of the dimensions and material density of the structural elements of the model. The mass of each payload is a measured value obtained by weighing the payload configuration provided for the tests. The stiffness characteristics of the model were provided by the manufacturer and are presented in figure 6.

The three payloads representing masses of 5000 lbm (2268 kg), 26 000 lbm (11 790 kg), and 45 000 lbm (20 410 kg) full scale were not models of any known prototype design but provided a means to study the effect of payload mass on the vibration response of the model structure.

Suspension System

During the vibration tests, the model configuration was suspended in a cable and spring system which offered negligible restraint against oscillatory motion in the lateral planes. Rigid-body frequencies of the model-cable system were at least one decade below the lowest structural modes. The suspension, shown schematically in figure 7, consisted of cable supports on both sides of the model. On each side of the structure one end of the cable was attached directly to the solid rocket motor casing near the level of the forward shear ties. The other end passed through an overhead pulley and terminated at a leaf spring located near the base of the model. The model elevation was adjustable with the use of hand winches placed at the leaf spring end of the cable to compensate for elongation of the support cables caused by different fuel loading conditions.

Shaker System

Excitation of the model was accomplished by use of a set of eight matched electromagnetic shakers each rated at 50 vector force pounds (222.4 N). The shakers were suspended from overhead by cables to eliminate support resonances and to permit nearly unrestricted choice of the location of shaker attachment points on the model. All shakers were attached to the model by a vacuum-type attachment which also permitted versatility in choosing shaker attachment locations. A diagram showing the total number of shaker locations for the model in the pitch and yaw planes is shown in figure 8. Some of the suspended shakers used to excite the model in the yaw plane may be seen in figure 2. Each

shaker was powered by an individual amplifier, but frequency of excitation on all shakers was simultaneously controlled by a common oscillator. Operation of the shaker system was centralized at a control panel which allowed the use of one or more shakers at the same time. The control panel was equipped with four dual-beam oscilloscopes on which the armature voltage and current of any shaker could be monitored. A switching arrangement was provided so that on any scope the phase of the voltage or current of a shaker armature could be observed relative to the phase of the velocity or current of the armature of any other shaker. This arrangement enabled a check of the phase relationship between the different shakers used in exciting a particular mode. The control panel also contained phase switches which could change the phase of each shaker by 180^{o}. Finally, a master switch was installed which allowed a simultaneous termination of power to all shakers in operation. This switch was used to remove the excitation force to obtain records of the decay of the model oscillation during the transient phase of the response.

Instrumentation

The mode shapes and frequencies at resonances of the model were determined with the use of two movable probes. The probes were crystal-type accelerometers coupled with a cathode follower and amplifier as signal conditioning equipment. In addition, a crystal-type force gage was linked in the arm of the shaker attachment at $x/l = 0.934$ in order that the shaker excitation force could be measured. A schematic diagram of this instrumentation system is shown in figure 9. The accelerometers and force gage were calibrated through their respective signal conditioning systems and were found to have a flat response from 6 Hz to above 100 Hz.

Test Procedure

Oscillation of the model in the pitch and yaw directions was induced to obtain resonant frequencies and associated mode patterns for the test condition shown in table IV.

TABLE IV.- SUMMARY OF MODEL TEST CONDITIONS

Nominal payload		Flight time, sec	Excitation direction
lbm	kg		
5 000	2 268	0, 53, 105	Pitch, yaw
26 000	11 790	0, 105	Pitch, yaw
45 000	20 410	0, 53, 105	Pitch, yaw

In tuning the modes for different fuel loading conditions of the model, several combinations of shakers were required; however, the following description reviews the general procedure followed in exciting modes for all loading conditions. The shaker in the

location estimated to provide the maximum model excitation was used to excite the mode. The Lissajous figure for the variation of shaker armature current with voltage (variation of velocity with force) was displayed on the monitoring oscilloscope and the frequency adjusted until the current and voltage were in phase. Traces of the decay of the model deflection response were recorded in order that the decay frequency could be compared with the forcing frequency to ascertain accurate tuning of the mode. Other needed shakers were sequentially energized and shaker amplitude, polarity, and frequency were adjusted to insure that the shaker force was in phase with velocity at all points of excitation on the model. In addition, for the shaker located at $x/l = 0.934$ where the force gage was linked in the shaker arm, the variation of shaker force with velocity was also monitored.

Mode shapes were measured with the use of a fixed and a movable probe by noting the amplitude and phase at various points on the model relative to a chosen antinode location for the particular mode. The amplified signals from these accelerometers were filtered to eliminate signal noise and were fed into an oscilloscope displaying a Lissajous figure normalized at a 45° slope at the location of the fixed accelerometer. A transparent circular plastic face calibrated in tangents and attached to the front of the oscilloscope screen permitted direct reading of the amplitude and phase. Therefore, by moving the accelerometer to different locations on the model, the amplitude and phase of the response at any location on the model relative to the location of the fixed accelerometer was read directly from the scope face.

RESULTS AND DISCUSSION

The measured and computed vibration characteristics are presented for representative payloads and flight conditions. Experimental results typical of the launch-vehicle response are compared with computed results and specific areas of disagreement are discussed in detail. To avoid unnecessary repetition of data, experimental and computed mode shapes are presented in the same figures. All mode shape data are shown in figures 10 to 17 and associated frequencies in table V; however, the vibration data are discussed in the appropriate order under the following headings.

Experimental Modes

The experimental mode shapes and associated resonant frequencies were obtained for the test conditions shown in table IV for the tank pressures and propellant masses given in table VI. The experimental mode data presented in this paper are limited to typical examples of lateral response which represent the first three lateral modes for all propellant loading conditions and payload masses. These typical examples of measured mode shapes are shown for the intermediate weight 26 000 lbm (11 790 kg) payload.

TABLE V.- COMPARISON OF MEASURED AND COMPUTED FREQUENCIES

Type of frequency	Frequency, Hz, for flight times of –																	
	0 sec for –						53 sec for –						105 sec for –					
	Pitch			Yaw			Pitch			Yaw			Pitch			Yaw		
	Mode 1	Mode 2	Mode 3	Mode 1	Mode 2	Mode 3	Mode 1	Mode 2	Mode 3	Mode 1	Mode 2	Mode 3	Mode 1	Mode 2	Mode 3	Mode 1	Mode 2	Mode 3
Payload of 5000 lbm (2268 kg)																		
Experimental modes, f_e	8.7	13.0	31.1	8.4	13.2	21.7	9.1	14.2	26.7	9.3	14.5	20.1	10.3	19.8	30.8	10.6	18.7	24.2
Coupled modes utilizing unmodified outrigger coefficients, f_c	8.9	16.2	39.6	7.4	13.3	15.9							10.6	23.3	33.9	9.2	14.9	22.4
Coupled modes utilizing modified outrigger coefficients, f_c*	8.2	13.6	37.0	7.4	13.2	15.9	8.6	14.7	28.5	8.7	14.4	21.6	9.6	20.6	32.8	9.2	14.9	22.5
Uncoupled modes utilizing modified outrigger coefficients, f_u							8.6	14.7	28.5	8.2	14.4	21.6						
Payload of 26 000 lbm (11 790 kg)																		
Experimental modes, f_e	6.0	12.7	20.3	5.8	12.0	18.9							7.5	16.2	25.8	7.5	15.4	24.5
Coupled modes utilizing unmodified outrigger coefficients, f_c	6.2	15.6	20.7	5.5	12.2	21.4							7.7	18.3	31.6	7.1	15.9	30.1
Coupled modes utilizing modified outrigger coefficients, f_c*	5.9	12.6	20.6	5.5	12.2	21.4							7.3	15.9	29.3	7.1	15.9	30.1
Uncoupled modes utilizing modified outrigger coefficients, f_u	5.9	12.6	20.7	5.5	12.8	21.4							7.2	15.9	29.3	7.1	15.9	30.1
Payload of 45 000 lbm (20 410 kg)																		
Experimental modes, f_e	5.6	12.7	20.3	5.4	12.0	18.4	6.1	13.6	20.6	6.2	13.3	19.2	7.3	16.2	25.9	7.3	15.5	24.2
Coupled modes utilizing unmodified outrigger coefficients, f_c	5.8	15.6	20.5	5.1	12.2	21.2							7.3	18.2	31.2	6.8	15.8	29.7
Coupled modes utilizing modified outrigger coefficient, f_c*	5.5	12.5	20.5	5.1	12.2	21.2	6.0	13.3	21.3	5.6	13.2	20.7	7.0	15.8	27.1	6.8	15.8	29.7
Uncoupled modes utilizing modified outrigger coefficients, f_u	---	----	----	---	----	----	6.0	13.3	21.3	5.6	13.2	20.7						

TABLE VI.- TANK PRESSURE AND PROPELLANT LOADINGS

(a) Tank pressure

Flight time, sec	Tank pressure* for –							
	Oxidizer				Fuel			
	Stage I		Stage II		Stage I		Stage II	
	lb/in^2	N/cm^2	lb/cm^2	N/cm^2	lb/cm^2	N/cm^2	lb/in^2	N/cm^2
105	7.0	4.8	9.0	6.2	8.2	5.7	9.4	6.5
53	7.0	4.8	9.0	6.2	8.2	5.7	9.4	6.5
0	7.0	4.8	9.0	6.2	8.2	5.7	9.4	6.5

(b) Propellant loadings

Flight time, sec	Solid and liquid propellant loading for –											
	Stage II				Stage I				Stage 0*		Thrust vector control**	
	Oxidizer		Fuel		Oxidizer		Fuel		Solid**		Tank**	
	lbm	kg	lbm	kg	lbm	kg	lbm	kg	lbm	kg	lbm	kg
105	343.7	155.9	192.7	87.4	1321.1	599.2	689.5	312.8	0	0	0	0
53	343.7	155.9	192.7	87.4	1321.1	599.2	689.5	312.8	1650.0	748.4	62.0	28.1
0	343.7	155.9	192.7	87.4	1321.1	599.2	689.5	312.8	3300.0	1496.9	129.3	58.6

*Only stage I and stage II tanks require pressurization.

**Above loadings are for individual tanks.

The pitch and yaw responses for lift-off (t = 0) are shown in figures 12 and 13, respectively; and the asymmetric solid rocket motor pitch response is shown in figure 14. (Modes are considered symmetric if the motions of the solid rocket motors are in phase as indicated in fig. 5.) Corresponding lateral mode response at solid rocket motor burnout (t = 105 sec) is shown in figures 15 to 17. In general, the motions for symmetric modes of the two solid rocket motors were coincident as indicated by the experimental deflection patterns in figures 12, 13, 15, and 16. At numerous stations on the model core, the displacements (figs. 12, 13, 15, and 16) were measured on the front (circular symbol) and back (square symbol) of the structure to indicate localized response and thus avoid giving a distorted view of the beam-type lateral motion.

Theoretically, lightly damped structures at resonance have mode shapes which are orthogonal. (Structural damping ratios observed during decay tests in the model were very low in the order of 1 percent critical damping; that is, $g = 2\frac{c}{c_r} = 0.02$.) The accuracy of the symmetric experimental mode shapes is, therefore, indicated by computation of the generalized masses by utilizing all modes including rigid body translation and rotation. The generalized masses obtained by using the measured mode shapes presented in this report were computed from the mass data given in table I and are shown in tables VII and VIII as normalized generalized mass matrices. The elements of the generalized mass matrix M_{ij} were calculated by use of the equation:

$$\left.\begin{aligned} M_{ij} &= \sum_{q=1}^{N} y_i(x_q) y_j(x_q) m_q = M_{ii} \qquad (i = j) \\ M_{ij} &= \sum_{q=1}^{N} y_i(x_q) y_j(x_q) m_q \approx 0 \qquad (i \neq j) \end{aligned}\right\} \tag{8}$$

where

m_q mass located at station x_q

$y_i(x_q)$ ith modal displacement function evaluated at x_q

$y_j(x_q)$ jth modal displacement function evaluated at x_q

TABLE VII.- ORTHOGONALITY CHECK OF EXPERIMENTAL MODE SHAPES

[t = 0, 26 000 lbm (11 790 kg) payload]

(a) Pitch

Elements of generalized mass matrix			
Mode	Frequency, Hz	M_{ii}	
		lbm	kg
Rigid body translation	0	11 032.0	5004.0
Rigid body rotation	0	962.2	436.4
Mode 1	6.0	368.9	167.3
Mode 2	12.7	1 941.1	880.5
Mode 3	20.3	543.7	246.6

Normalized generalized mass matrix

1.000	0.002	-0.028	0.044	-0.012
0.002	1.000	0.019	0.032	-0.032
-0.028	0.019	1.000	-0.102	-0.034
0.044	0.032	-0.102	1.000	0.073
-0.012	-0.032	-0.034	0.073	1.000

(b) Yaw

Elements of generalized mass matrix			
Mode	Frequency, Hz	M_{ii}	
		lbm	kg
Rigid body translation	0	11 032.0	5004.0
Rigid body rotation	0	962.2	436.4
Mode 1	5.8	277.8	126.0
Mode 2	12.0	860.0	390.1
Mode 3	18.9	775.9	351.9

Normalized generalized mass matrix

1.000	0.002	-0.021	0.027	0.006
0.002	1.000	0.068	-0.001	-0.008
-0.021	0.068	1.000	0.134	-0.118
0.027	-0.001	0.134	1.000	0.184
0.006	-0.008	-0.118	0.184	1.000

TABLE VIII.- ORTHOGONALITY CHECK OF EXPERIMENTAL MODE SHAPES

[t = 105 seconds, 26 000 lbm (11 790 kg) payload]

(a) Pitch

Elements of generalized mass matrix			
Mode	Frequency, Hz	M_{ii}	
		lbm	kg
Rigid body translation	0	4123.4	1870.3
Rigid body rotation	0	700.4	317.7
Mode 1	7.5	383.9	174.0
Mode 2	16.2	1134.1	514.4
Mode 3	25.8	937.6	425.3

Normalized generalized mass matrix

1.000	-0.001	-0.083	0.012	0.114
-0.001	1.000	0.064	-0.022	0.068
-0.083	0.064	1.000	-0.070	0.052
0.012	-0.022	-0.070	1.000	-0.099
0.114	0.068	0.052	-0.099	1.000

(b) Yaw

Elements of generalized mass matrix			
Mode	Frequency, Hz	M_{ii}	
		lbm	kg
Rigid body translation	0	4123.4	1870.3
Rigid body rotation	0	700.4	317.7
Mode 1	7.5	325.0	147.4
Mode 2	15.4	1152.9	522.9
Mode 3	24.5	633.0	287.1

Normalized generalized mass matrix

1.000	-0.001	-0.047	-0.046	0.124
-0.001	1.000	0.038	-0.073	-0.030
-0.047	0.038	1.000	0.021	-0.038
-0.064	-0.073	0.021	1.000	-0.028
0.124	-0.030	-0.038	-0.028	1.000

The numbers tabulated under the heading "Elements of the generalized mass matrix" in tables VII and VIII are the $\overline{M}_{ij}$ terms computed from equations (8) and the model mass data and the measured mode shapes. The element of the normalized generalized mass matrix $\overline{M}_{ij}$ is defined by

$$\overline{M}_{ij} = \frac{M_{ij}}{\sqrt{M_{ii}}\sqrt{M_{jj}}}$$

Analytical Modes and Comparison With Experiment

At the beginning of this section a selected number of computed lateral modes which incorporate unmodified aft outrigger coefficients are presented. These computed data are compared with experimental results to indicate the need for modification of the aft outrigger joint fixity. If the modified aft outrigger coefficients in the coupled mathematical model are utilized, lateral modal data can then be presented for all propellant loading conditions and payload configurations. Longitudinal and torsional modes also obtained by using the modified aft outrigger coefficients in the coupled analysis are given for several representative cases. Additional computations (designated the uncoupled analysis) are discussed which show the effect of omitting inertial coupling due to mass eccentricity in the mathematical model.

Effect of outrigger flexibility on lateral modes.- Initially, analytical modes and frequencies were computed by using the unmodified flexibility coefficients of the aft outriggers identified previously. Typical examples of the lateral mode shapes, thus obtained, are compared with measured data in figures 10 and 11. Computed frequencies f_c are compared with measured values f_e for the two extreme propellant loading conditions in table V. In these comparisons of computed and measured mode shapes and frequencies, disagreement is significant in the second mode. The source of the discrepancy was traced to causes exhibited by two interesting features in the measured and computed mode shapes: The first is the difference in the slope of the core displacement pattern at the aft end of the structure and the second is the difference in the displacements of the solid rocket motors. (See figs. 10 and 11.) In these initially computed curves, the slope at the aft end of the core ($x/l = 0.942$) is in agreement with the slope of the solid rocket motion which reflects the assumed fixed restraint at the aft outrigger attachment against rotation of the solid motors in the pitch plane (that is, coefficients of $M'_{VII,SRM1}$ and $M'_{VII,SRM2}$) given in the appendix. The measured second mode shapes (figs. 10(b) and 11(b)), however, show the slopes of the core and solid motors to be nearly perpendicular and indicate that the fixed restraint used in the computation may be a misrepresentation of the actual behavior of the model at this point. (Note that the end experimental point in fig. 11(c) denotes motion of the stage I engine and does not indicate a reversal of slope of the aft end of the model core.)

The vibration data were, therefore, recomputed by using modified coefficients which assume a negligible restraint, approaching a pinned condition, against rotation of the solid motors in the pitch plane $\left(\text{that is, } M'_{VIII,SRM1} = M'_{VIII,SRM2} \approx 0\right)$. These data constitute the major results of the analytical effort and are presented and discussed in this section.

Lateral modes, coupled analysis.- Mode shapes were computed for all propellant loading conditions listed in table IV and for three payload masses; however, only a representative set having dominant motion in the pitch and yaw planes is included since a comparison of these results indicates, in general, the degree of agreement attained. This set of mode shapes is shown in figures 12 to 17 and were obtained for the 26 000 lbm (11 790 kg) payload at flight times $t = 0$ and $t = 105$ seconds. The computed displacements are compared with measured results on the basis of relative amplitude and location of nodes and are generally in satisfactory agreement with the measured results. As evident in figures 12 to 17, the results compare more favorably for the fundamental mode but compare progressively less favorably for higher modes. Poor agreement in computed and measured mode shapes occurred in only three of the 48 computations: the pitch and yaw third mode of the 5000 lbm (2268 kg) payload, $t = 0$ flight time, and the third yaw mode of the 45 000 lbm (20 410 kg) payload, $t = 53$ seconds flight time. These cases, although not shown, possessed qualitative similarity in computed and measured mode shapes but exhibited poor agreement in light of the amplitude-node location criteria used as a basis for comparison.

The computed natural frequencies associated with the mode shapes discussed are compared with measured resonant frequencies and are shown for all flight conditions and payload weights in table V. Computed frequencies utilizing modified outrigger coefficients are designated $f_c{}^*$ and experimentally determined values, f_e. As in the case of the mode-shape comparison, the computed coupled frequencies $f_c{}^*$ generally agree well with the measured values f_e for the first mode, but the results again compare less favorably at the higher modes. The deviation between f_e and $f_c{}^*$ for the first mode ranges from 0 to 15 percent, the greater number of these frequencies agreeing within 8 percent. Agreement in the second mode frequencies was also within 8 percent except for a maximum deviation of 20 percent in one case. The third-mode coupled frequencies deviate from the measured values by as much as 20 percent except for a 35-percent difference in measured and computed frequencies corresponding to the three mode shapes for the 5000 lbm (2268 kg), $t = 0$ yaw case already discussed.

Longitudinal and torsion modes, coupled analysis.- In addition to lateral response, the matrix Holzer analysis yields modes which exhibit dominantly longitudinal or torsion motion or solid-rocket-motor asymmetric yaw. These modes are shown qualitatively in figure 5 and are characterized as:

(1) Solid-rocket-motor symmetric longitudinal motion combined with core longitudinal motion (fig. 5(c))

(2) Solid-rocket-motor asymmetric pitch motions combined with core torsion motion (fig. 5(d))

(3) Solid-rocket-motor asymmetric yaw motion combined with core longitudinal motion (fig. 5(e))

(4) Solid-rocket-motor asymmetric longitudinal motion combined with core yaw motion (fig. 5(f)).

Experimental data were obtained only for the pitch-torsion modes. Symmetric longitudinal and asymmetric yaw motion was not observed during the tests since the experimental investigation was concerned primarily with lateral response of the three-body configuration. Consequently, comparison between measured and computed data is possible only for the pitch-torsion mode. Nevertheless, for completeness, the longitudinal and yaw frequencies given by the matrix Holzer coupled mathematical model for the 26 000 lbm (11 790 kg), $t = 0$ configuration are given in table IX.

TABLE IX.- COMPUTED FREQUENCY FOR LONGITUDINAL, YAW, AND PITCH MODES OF SOLID ROCKET MOTOR

[26 000 lbm (11 790 kg) payload]

Mode	Computed frequency, Hz, for –	
	$t = 0$ sec	$t = 105$ sec
SRM asymmetric yaw; core longitudinally (fig. 5(e))	13.7	44.3
SRM asymmetric longitudinally; core yawing (fig. 5(f))	17.3	36.3
SRM symmetric longitudinally; core longitudinally (fig. 5(c))	23.9	36.7
SRM asymmetric pitch; core in torsion (fig. 5(d))	15.3	29.8

The pitch-torsion mode was difficult to predict accurately for reasons somewhat similar to those given for the second pitch mode. A parametric study was made to determine the effect of the aft outrigger torsional flexibility coefficient on the pitch-torsion mode. It was found that in order to obtain agreement with measured results, the aft outrigger flexibility would have to approximate the flexibilities of the core and the forward

outriggers taken individually. By using recomputed coefficients, as indicated in table II, the results shown in figures 14 and 17 were obtained.

Coupled analysis compared with uncoupled analysis.- The matrix Holzer analysis permits the assumption that combined pitch-torsion motion may be uncoupled from combined yaw-longitudinal motion. Vibration data were computed by using the uncoupled version of the analysis to determine whether the added complexity of coupling produces results in better agreement with the measured data. Uncoupled frequencies for representative configurations are given in table V. Negligible variations were noted in comparable values of the coupled and uncoupled frequencies and indicated that the coupled and uncoupled versions of the analysis were equally successful in predicting the first three lateral modes of the model response.

CONCLUDING REMARKS

A matrix Holzer analysis employing a three-dimensional coupled mathematical model was used to compute the free vibration modes and frequencies of a three-body clustered launch vehicle. Computed data for the three lowest lateral pitch and yaw modes were obtained for propellant loading conditions of the model corresponding to flight times ranging from lift-off (time 0) to solid rocket burnout (time, 105 sec) and for payload masses corresponding to 5000 lbm (2268 kg), 26 000 lbm (11 790 kg), and 45 000 lbm (20 410 kg) full scale.

In general, the coupled mathematical model analysis adequately predicts the first three lateral vibration modes of the model configuration for all payload weights and propellant loading conditions. Agreement between the computed and measured data is good for the fundamental mode but becomes less favorable at higher modes.

The coupled system analytical data were computed by using aft outrigger attachment flexibilities reevaluated on the basis of experimental evidence. Computation of mode shapes and frequencies assuming a negligible restraint against rotation of the solid rocket motors in the pitch plane resulted in a decided improvement in agreement between the measured and computed pitch-mode response. This study indicates that correct treatment of intertank connections is critical for certain modes.

Mode shapes and associated resonant frequencies computed by the coupled system analysis were compared with corresponding measured data and other computed data obtained from analyses using an uncoupled mathematical model. The results indicate that an uncoupled analysis is sufficient for this three-body configuration.

Modes associated with dominantly longitudinal motion and yaw motion of the solid rocket motors were obtained analytically. Since no experimental data were available for comparison, the accuracy of these predictions was undetermined.

The use of dynamic models in an experimental test program in conjunction with an analytical study provides a valuable tool for accurate appraisal of the dynamic behavior of the physical vehicle. The experimental program provides an overall picture of the vehicle vibration characteristics and, in addition, can provide dynamic characteristics of the complex components of the model for which an accurate analysis is extremely difficult or impossible.

Langley Research Center,
National Aeronautics and Space Administration,
Langley Station, Hampton, Va., February 7, 1968,
124-08-05-22-23.

APPENDIX

TRANSFER MATRICES USED IN ANALYSIS

The analytical procedure outlined in the main body of the present paper follows closely the analysis presented in section IC-1 of reference 6. The transfer matrices for the elemental massless rods and lumped masses employed herein differ somewhat from those presented in reference 6 and are therefore discussed in this appendix. Relationships defining the outrigger flexibility coefficients are based on a sign convention which also differs from that of reference 6. Since these equations are used in the digital program written by the authors of reference 6, they are included in this appendix.

Symbols

a	length of aft truss
b	eccentricity of aft truss, 2.6 in. (6.6 cm)
EA(x)	longitudinal-stiffness distribution
EI(x)	yaw-bending-stiffness distribution
EI'(x)	pitch-bending-stiffness distribution
e	eccentricity of mass center of gravity relative to cross-sectional centroid
GJ(x)	torsional-stiffness distribution
I_o	bending inertia of branch mass about its own center of gravity
I_ϕ	bending inertia of lumped mass excluding flexible branch
$\bar{I}_\phi$	effective bending inertia of lumped mass including branch
I_t	torsional inertia
KAG(x)	shear stiffness distribution
K_B	rotational spring for branch mass

APPENDIX

L	length of massless rod element
l	distance from center line of core to center line of solid rocket motor (SRM)
m_{Bi}	ith flexibly attached branch mass
$\overline{m}_{Bi}$	effective lumped mass including branch mass
m_i	ith rigidly attached lumped mass
m_{li}	mass effective for longitudinal motion
P_1, P_2	aft outrigger joints for solid rocket motors 1 and 2, respectively
r	overhang distance of branch mass
S_B	first mass moment of branch mass
S_{ϕ_i}	first moment of ith mass excluding branch mass
ω	circular frequency of complete system
ω_B	rotational circular frequency of flexible branch mass
ω_{Bn}	rotational circular frequency of flexible branch mass with $I_O = 0$

Matrices:

$\{\ \}$	denotes column matrix
$[\ ]$	denotes square or rectangular matrix
$[A]$	flexibility matrix for pitch-torsion motion of forward outrigger
$[B]$	flexibility matrix for yaw bending motion of forward outrigger
$[C]$	flexibility matrix for pitch-torsion motion of aft outrigger
$[D]$	flexibility matrix for yaw-longitudinal motion of core at aft outrigger

APPENDIX

$[E]$ flexibility matrix for yaw-longitudinal motion of solid rocket motor and aft outrigger

$[E_b]$ submatrix of elastic matrix for yaw bending

$[E'_b]$ submatrix of elastic matrix for pitch bending

$[E_l]$ submatrix of elastic matrix for longitudinal deformation

$[E_t]$ submatrix of elastic matrix for torsional deformation

$[M_b]$ submatrix of mass matrix for yaw masses

$[M'_b]$ submatrix of mass matrix for pitch masses

$[M_l]$ submatrix of mass matrix for longitudinal masses

$[M_t]$ submatrix of mass matrix for torsional inertias

Vectors:

$\longrightarrow$ denotes force and linear displacement vectors

$\longrightarrow\!\!\!\!\!\!\rightarrow$ denotes moment and angular displacement vectors

Transfer Matrix for Massless Rods

The matrix which expresses the relationship between the internal loads and displacements at the ith and $i + 1$ stations across a massless rod is found from the static solution of the beam equations. The rods were assumed to have constant section properties in reference 6. In the present paper, however, provisions were made to allow for variable cross-sectional properties between the lumped masses. The matrix elements as given are generalizations of those of equation (1) on page 10 of reference 6 and reduce to them for constant cross-sectional properties. The mass and elastic transfer matrices are related to the beam elements as shown in sketch 1.

APPENDIX

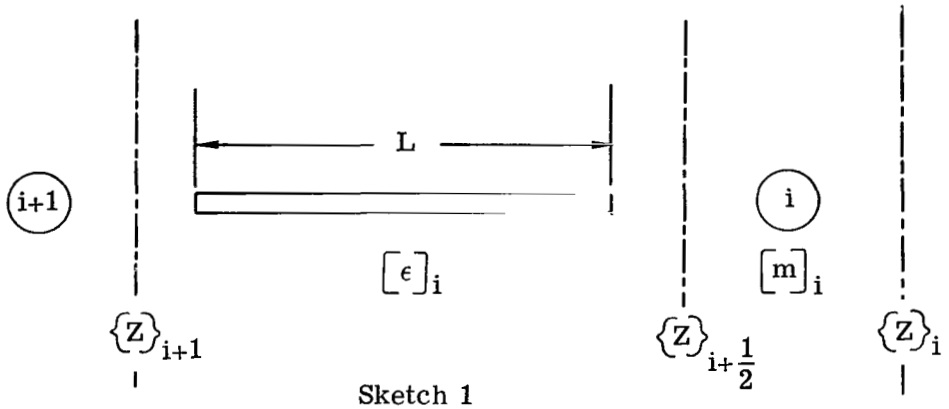

Sketch 1

By definition,

$$\{Z\}_{i+\frac{1}{2}} = [m]_i \{Z\}_i$$

$$\{Z\}_{i+1} = [\epsilon]_i \{Z\}_{i+\frac{1}{2}}$$

where

$$[\epsilon]_i = \left[\begin{array}{c|c|c|c} [E_b] & 0 & 0 & 0 \\ \hline 0 & [E_b'] & 0 & 0 \\ \hline 0 & 0 & [E_t] & 0 \\ \hline 0 & 0 & 0 & [E_l] \end{array}\right]_i$$

and

$$[E_b] = \left[\begin{array}{c|c|c|c} 1 & 0 & 0 & 0 \\ \hline L & 1 & 0 & 0 \\ \hline \int_0^L \frac{x}{E\bar{I}(x)}\,dx & \int_0^L \frac{dx}{E\bar{I}(x)} & 1 & 0 \\ \hline \int_0^L \frac{(L-x)x}{E\bar{I}(x)}\,dx - \int_0^L \frac{dx}{KAG(x)} & \int_0^L \frac{(L-x)}{E\bar{I}(x)}\,dx & L & 1 \end{array}\right]_i$$

APPENDIX

$$\left[E_t\right]_i = \begin{bmatrix} 1 & 0 \\ -\int_0^L \frac{dx}{GJ(x)} & 1 \end{bmatrix}_i$$

$$\left[E_\ell\right]_i = \begin{bmatrix} 1 & 0 \\ -\int_0^L \frac{dx}{AE(x)} & 1 \end{bmatrix}_i$$

Transfer Matrices for Lumped Masses

The elements of the mass transfer matrices in reference 6 were derived for configurations shown in sketch 2(a) where the ith mass m_i may be comprised of one mass, rigidly attached to the main beam with a mass m_B spring mounted to it. In this paper, the transfer matrices were modified to include configurations where mass m_B might be flexibly attached to m_i as indicated in sketch 2(b). The physical properties are obtained either theoretically, or as is often the case with complex mountings, from experimental data. Measured characteristics were employed for the 5000 lbm (2268 kg) payload analyses and were found to have a significant effect on both calculated frequencies and mode shapes. Expressions for the branch mass matrix elements are given. It should be noted that the branch need not be a lumped mass and spring but may be a multimass system representable with a single degree of freedom. It must nevertheless be attached to the main beam in a statically determinate manner.

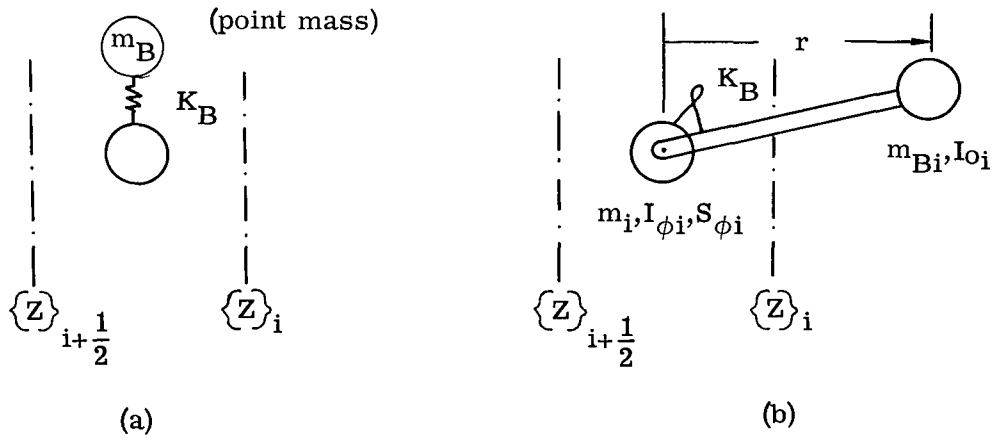

Sketch 2

APPENDIX

$$
[m]_i = \left[\begin{array}{cccc:cccc:cc:cc}
 & & & & & & & & 0 & \omega^2 me & 0 & 0 \\
 & & & & & & & & 0 & 0 & 0 & -\omega^2 me' \\
 & & [M_b] & & & & [0] & & 0 & 0 & 0 & 0 \\
 & & & & & & & & 0 & 0 & 0 & 0 \\
\hdashline
 & & & & & & & & 0 & \omega^2 me' & 0 & 0 \\
 & & & & & & & & 0 & 0 & 0 & \omega^2 me \\
 & & [0] & & & & [M_b'] & & 0 & 0 & 0 & 0 \\
 & & & & & & & & 0 & 0 & 0 & 0 \\
\hdashline
0 & 0 & 0 & \omega^2 me & 0 & 0 & 0 & \omega^2 me & & & 0 & 0 \\
0 & 0 & 0 & 0 & 0 & 0 & 0 & 0 & & [M_t] & 0 & 0 \\
\hdashline
0 & 0 & \omega^2 me' & 0 & 0 & 0 & -\omega^2 me' & 0 & 0 & 0 & & \\
0 & 0 & 0 & 0 & 0 & 0 & 0 & 0 & 0 & 0 & & [M_\ell] \\
\end{array}\right]
$$

where

$$
[M_b]_i = \begin{bmatrix} 1 & 0 & -\omega^2 \bar{S}_{\phi_i} & \omega^2 \bar{m}_i \\ 0 & 1 & -\omega^2 \bar{I}_{\phi_i} & \omega^2 S^*_{\phi_i} \\ 0 & 0 & 1 & 0 \\ 0 & 0 & 0 & 1 \end{bmatrix}
$$

$$
[M_b']_i = \begin{bmatrix} 1 & 0 & -\omega^2 \bar{S}_{\phi_i} & \omega^2 \bar{m}_i \\ 0 & 1 & -\omega^2 \bar{I}_{\phi_i} & \omega^2 S^*_{\phi_i} \\ 0 & 0 & 1 & 0 \\ 0 & 0 & 0 & 1 \end{bmatrix}
$$

$$
[M_t]_i = \begin{bmatrix} 1 & \omega^2 I_{ti} \\ 0 & 1 \end{bmatrix}
$$

APPENDIX

$$\left[M_{\ell}\right]_i = \begin{bmatrix} 1 & \omega^2 m_{\ell i} \\ 0 & 1 \end{bmatrix}$$

and

$$\bar{S}_{\phi_i} = S_{\phi_i} + \frac{S_{B_i}}{1 - \left(\frac{\omega}{\omega_B}\right)^2}$$

$$S^*_{\phi_i} = S_{\phi_i} + S_{B_i}\left[\frac{1}{1 - \left(\frac{\omega}{\omega_B}\right)^2}\right]$$

$$\bar{I}_{\phi_i} = I_{\phi_i} + \frac{\left(m_B r^2 + I_o\right)}{1 - \left(\frac{\omega}{\omega_B}\right)^2}$$

$$\bar{m}_i = m_i + m_{B_i}\left[1 + \frac{\left(\frac{\omega}{\omega_{B_n}}\right)^2}{1 - \left(\frac{\omega}{\omega_B}\right)^2}\right]$$

$$S_{B_i} = m_{B_i} r$$

$$\omega_{B_n} = \sqrt{\frac{K_B}{m_{B_i} r^2}}$$

$$\omega_{B_i} = \sqrt{\frac{K_{B_i}}{m_{B_i} r^2 + I_{o_i}}}$$

Outrigger Flexibility Coefficients

Transfer matrices representing the forward and aft outriggers (which are assumed to be massless) are obtained from flexibility relationships between loads and displacements. At the forward attachment which cannot transmit bending moments or longitudinal

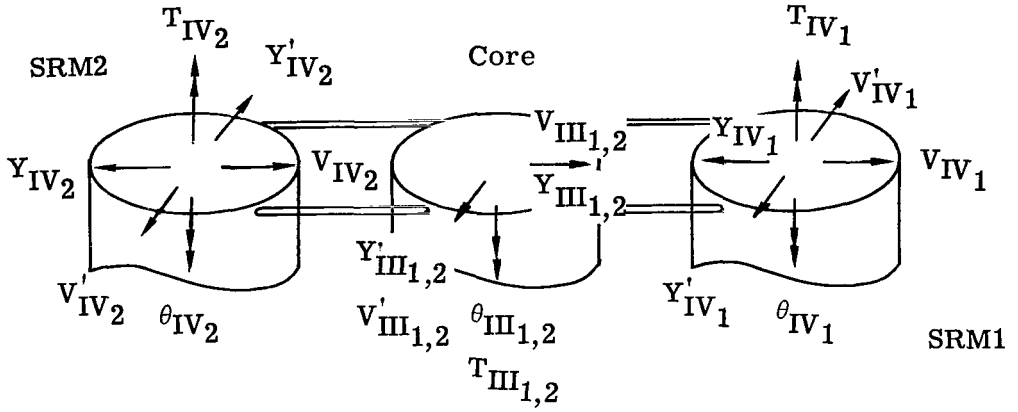

Sketch 3

forces, a static analysis employing the sign conventions indicated in the accompanying diagrams yields the following expressions:

$$\begin{Bmatrix} Y'_{IV_1} - Y'_{III_1} - \theta_{III}\ell \\ \theta_{IV_1} - \theta_{III_1} \\ Y'_{IV_2} + Y'_{III_2} - \theta_{III_2} \\ \theta_{IV_2} - \theta_{III_2} \end{Bmatrix} = [A] \begin{Bmatrix} -V'_{IV_1} \\ -T_{IV_1} \\ -V'_{IV_2} \\ -T_{IV_2} \end{Bmatrix}$$

for pitch bending-torsion motion (see ref. 6, p. 22) and

$$\begin{Bmatrix} Y_{IV_1} - Y_{III_1} \\ -Y_{IV_2} - Y_{III_2} \end{Bmatrix} = [B] \begin{Bmatrix} -V_{IV_1} \\ V_{IV_2} \end{Bmatrix}$$

for yaw bending motion (see ref. 6, p. 23). Subscripts 1 and 2 denote solid rocket motors 1 and 2, respectively.

At the aft outrigger, the following pitch-torsion load deflection relationships (eq. (14) in ref. 6, p. 28) are derived:

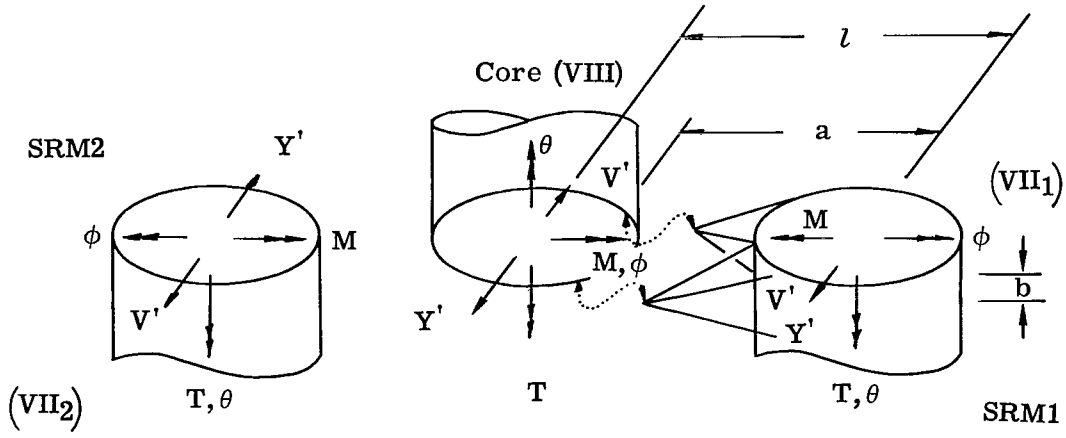

Sketch 4

$$\begin{Bmatrix} Y' \\ \theta \\ \phi' \\ \hline Y' \\ \theta \\ -\phi' \end{Bmatrix}_{VII_2} + \begin{bmatrix} -1 & -l & b \\ 0 & -1 & 0 \\ 0 & 0 & -1 \\ 1 & -l & -b \\ 0 & -1 & 0 \\ 0 & 0 & -1 \end{bmatrix} \begin{Bmatrix} Y' \\ \theta \\ \phi' \end{Bmatrix}_{V_{III}} = [C] \begin{Bmatrix} V' \\ T \\ M' \\ \hline V' \\ T \\ -M' \end{Bmatrix}_{VII_2}$$

Yaw-longitudinal properties at the aft outrigger are based on the core flexibility and the truss-solid rocket motor flexibilities considered separately. This treatment is necessitated by the fact that zero yaw bending moment is transmitted at joints P_1 and P_2, whereas all other attachment joints are assumed to be fixed. From the following schematic,

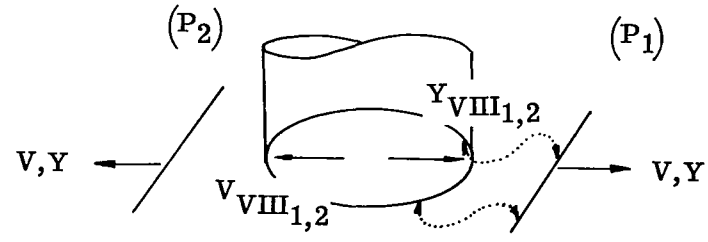

Sketch 5

consideration of core flexibility (see ref. 6, pp. 16-17 and pp. 30-31) leads to

$$\begin{Bmatrix} Y \\ \xi \\ --- \\ Y \\ \xi \end{Bmatrix}_{P_2}^{P_1} = [D] \begin{Bmatrix} \phi \\ Y \\ \phi' \\ Y' \\ \theta \\ \xi \\ --- \\ V \\ --- \\ V \end{Bmatrix}_{VII_2}^{VII_1}{}^{VIII}$$

and truss solid rocket motor flexibility (see eq. (15) in ref. 6, pp. 29-30) leads to

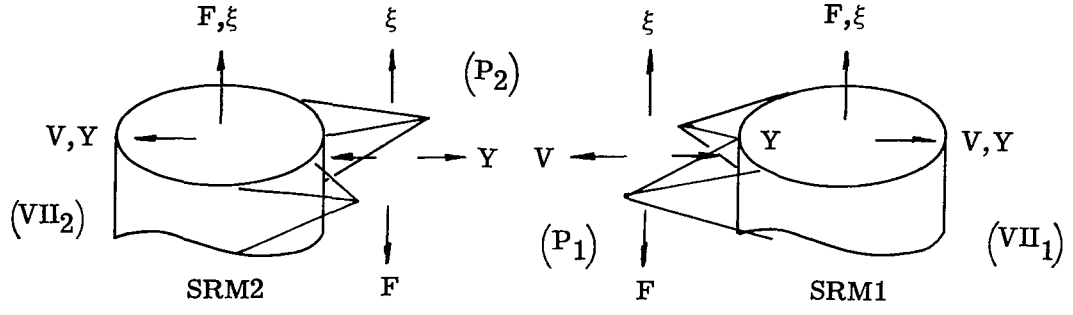

Sketch 6

$$\begin{Bmatrix} \xi \\ Y \\ --- \\ \xi \\ Y \end{Bmatrix}_{P_2}^{P_1} - \begin{Bmatrix} \xi \\ Y \\ --- \\ \xi \\ Y \end{Bmatrix}_{VII_2}^{VII_1} + \begin{Bmatrix} -(l-a) \\ 0 \\ l-a \\ 0 \end{Bmatrix} \phi_{VIII} - \begin{Bmatrix} a \\ -b \\ --- \\ -a \\ -b \end{Bmatrix}_{\phi_{VIII_2}}^{\phi_{VIII_1}} = [E] \begin{Bmatrix} F \\ -V \\ --- \\ F \\ -V \end{Bmatrix}_{P_2}^{P_1}$$

It should be noted that transfer matrices for the forward and aft outriggers are never obtained explicitly. Certain relationships which would be contained therein are employed to obtain solutions for the intermediate unknowns of equation (4).

REFERENCES

1. Mixson, John S.; Catherine, John J.; and Arman, Ali: Investigation of the Lateral Vibration Characteristics of a 1/5-Scale Model of Saturn SA-1. NASA TN D-1593, 1963.

2. Catherine, John J.: Torsional Vibration Characteristics of a 1/5-Scale Model of Saturn SA-1. NASA TN D-2745, 1965.

3. Mixson, John S.; and Catherine, John J.: Comparison of Experimental Vibration Characteristics Obtained From a 1/5-Scale Model and From a Full-Scale Saturn SA-1. NASA TN D-2215, 1964.

4. Thompson, William M., Jr.: An Investigation of the Response of a Scaled Model of a Liquid Propellant, Multistage Launch Vehicle to Longitudinal Excitation. NASA TN D-3975, 1967.

5. Jaszlics, Ivan J.; and Morosow, George: Dynamic Testing of a 20% Scale Model of the Titan III. AIAA Symposium on Structural Dynamics and Aeroelasticity, Aug.-Sept. 1965, pp. 477-485.

6. Loewy, Robert G.; and Joglekar, Mukund M.: Matrix Holzer Analyses for Fully-Coupled Vibrations of Clustered Launch-Vehicle Configurations Including Applications to the Titan IIIC and Uncoupled Saturn I Cases. NASA CR-592, 1966.

7. Pestel, Edward C.; and Leckie, Frederick A.: Matrix Methods in Elastomechanics. McGraw-Hill Book Co., Inc., c.1963.

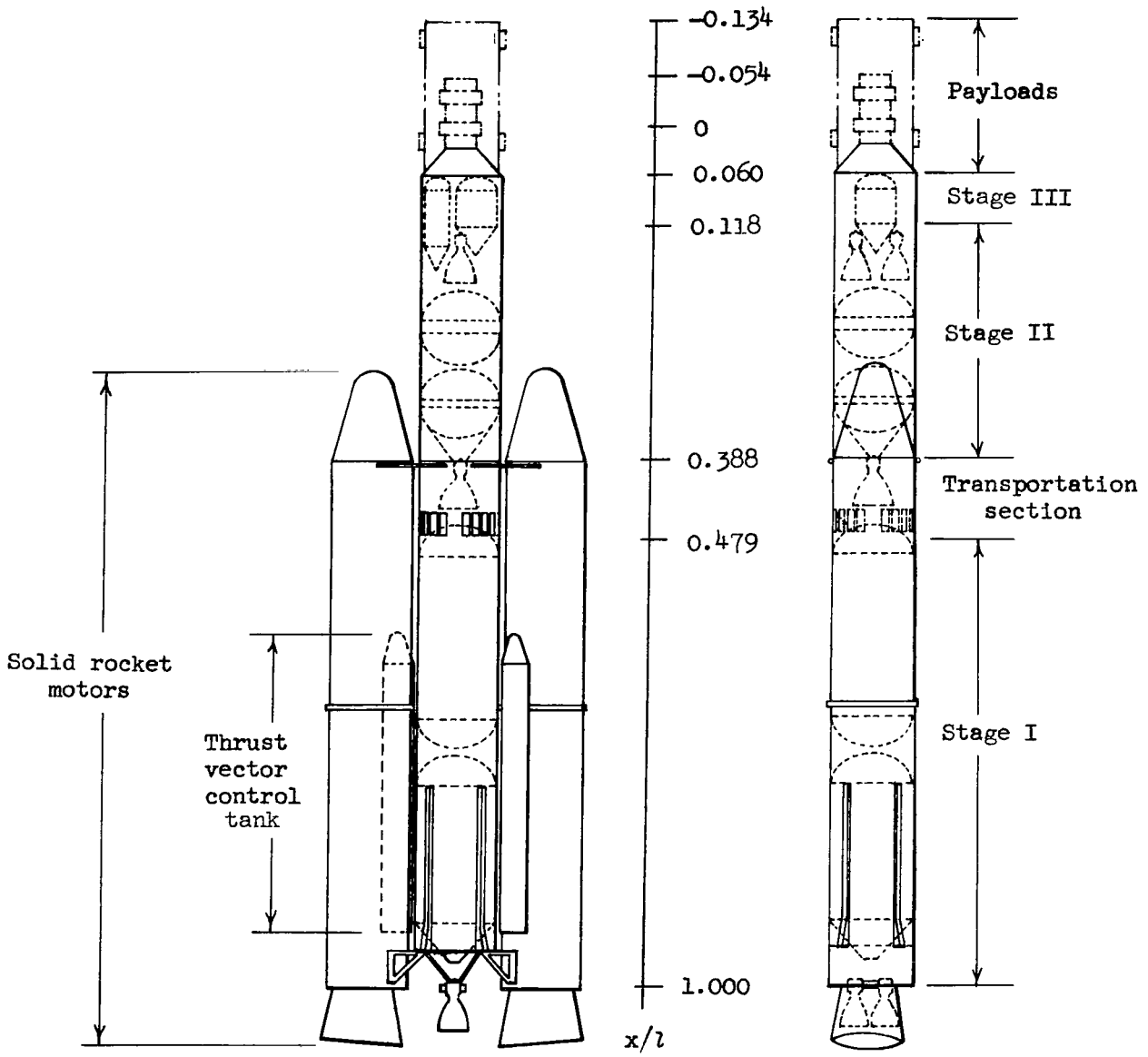

Figure 1.- Components of model configuration.

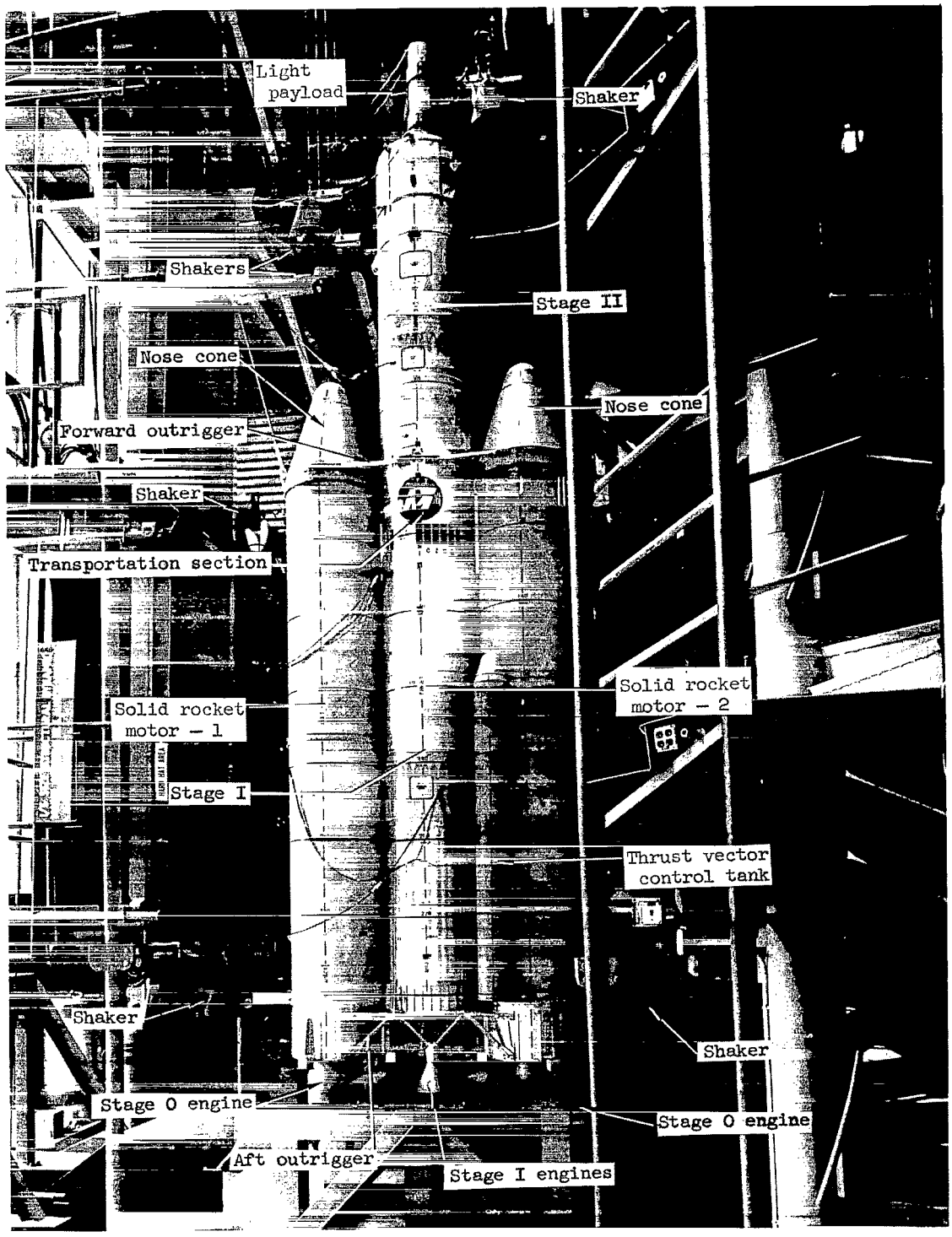

Figure 2.- Model configuration in yaw test position.

L-64-6652.1

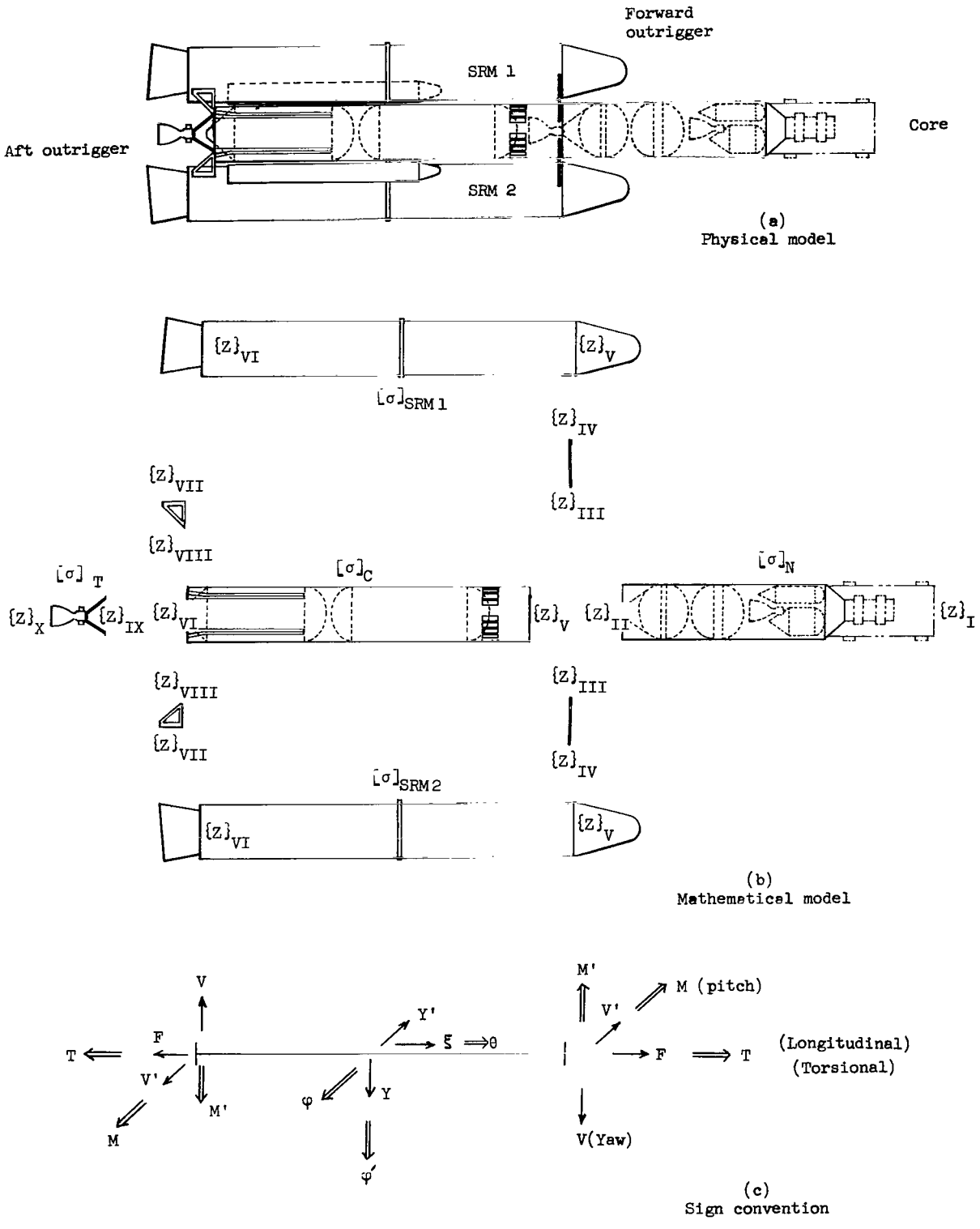

Figure 3.- Mathematical model.

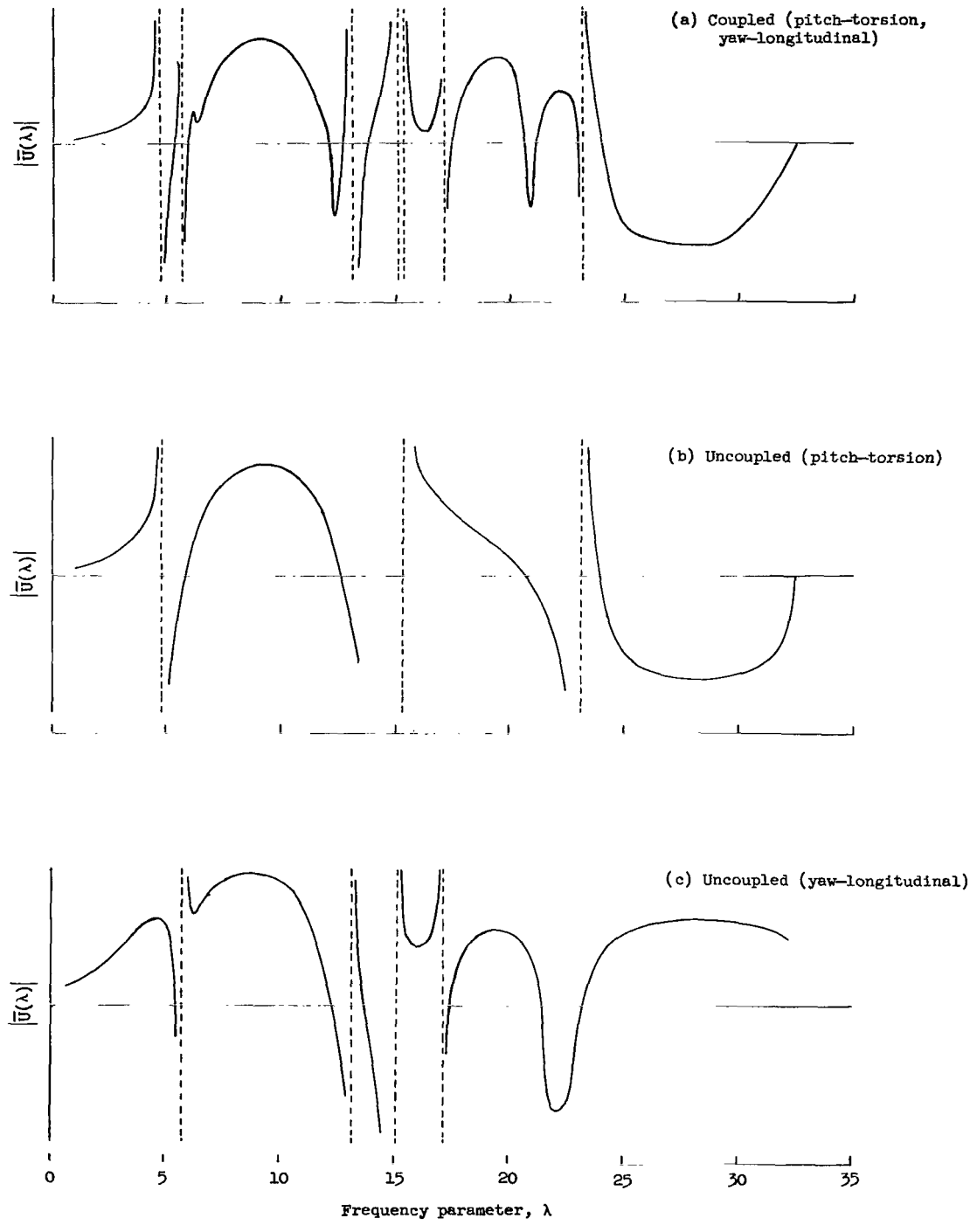

Figure 4.- Variation of nondimensional $|\overline{U}(\lambda)|$ with frequency parameter λ. Curves determined from matrix Holzer analysis computed for coupled and uncoupled mathematical model.

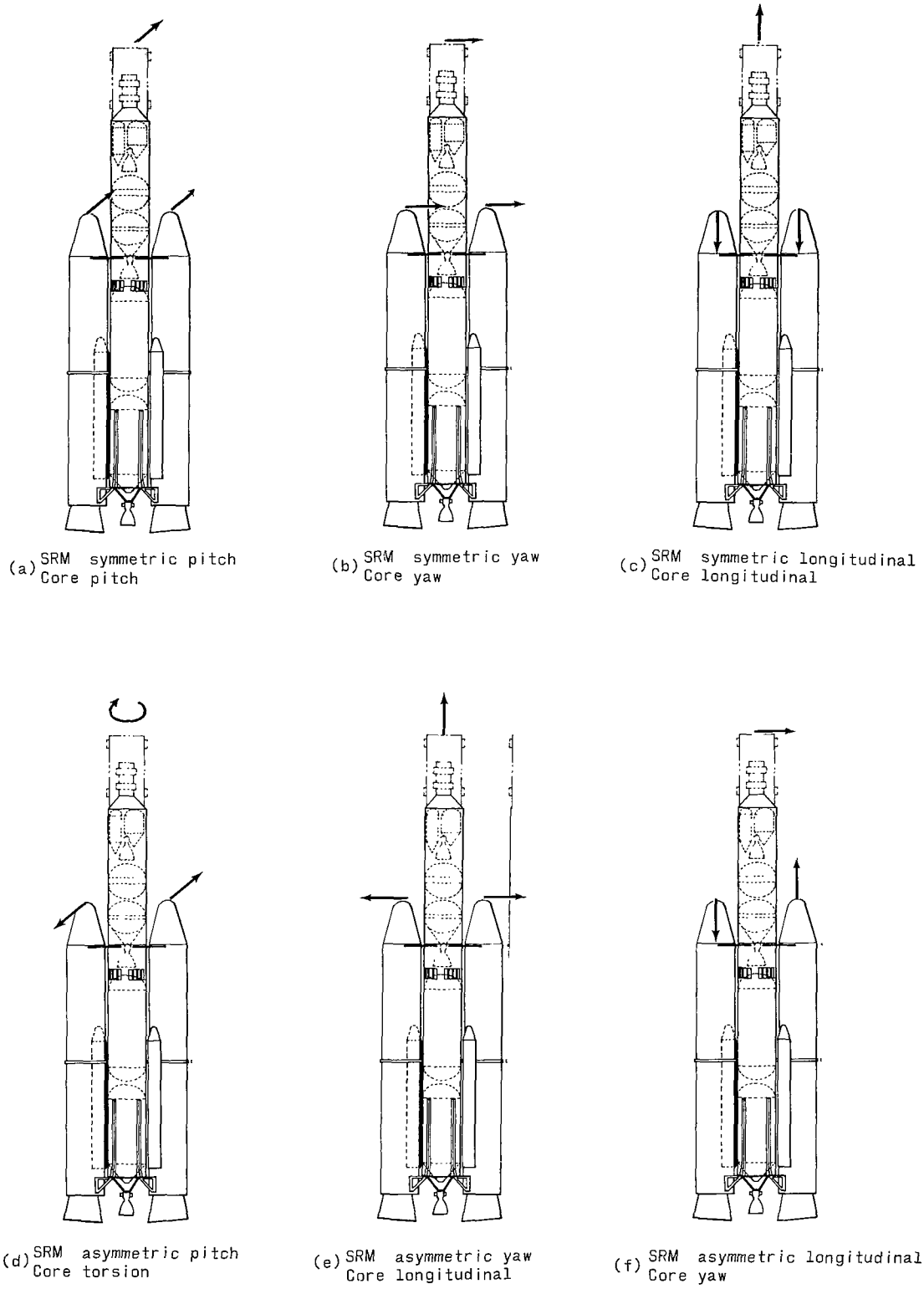

Figure 5.- Qualitative description of modal deflection for system with negligible intermodal coupling.

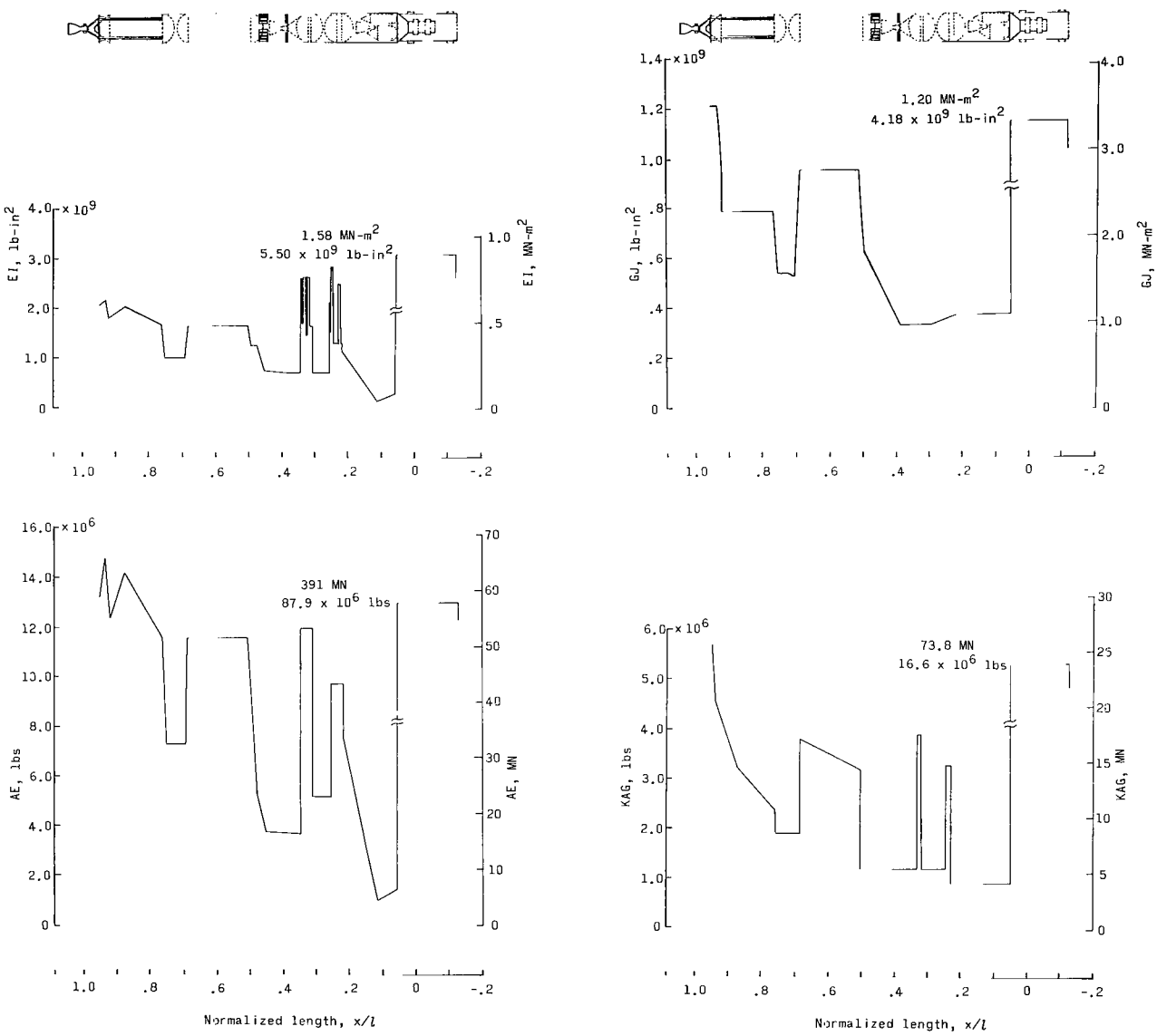

(a) Core.

Figure 6.- Model stiffness data.

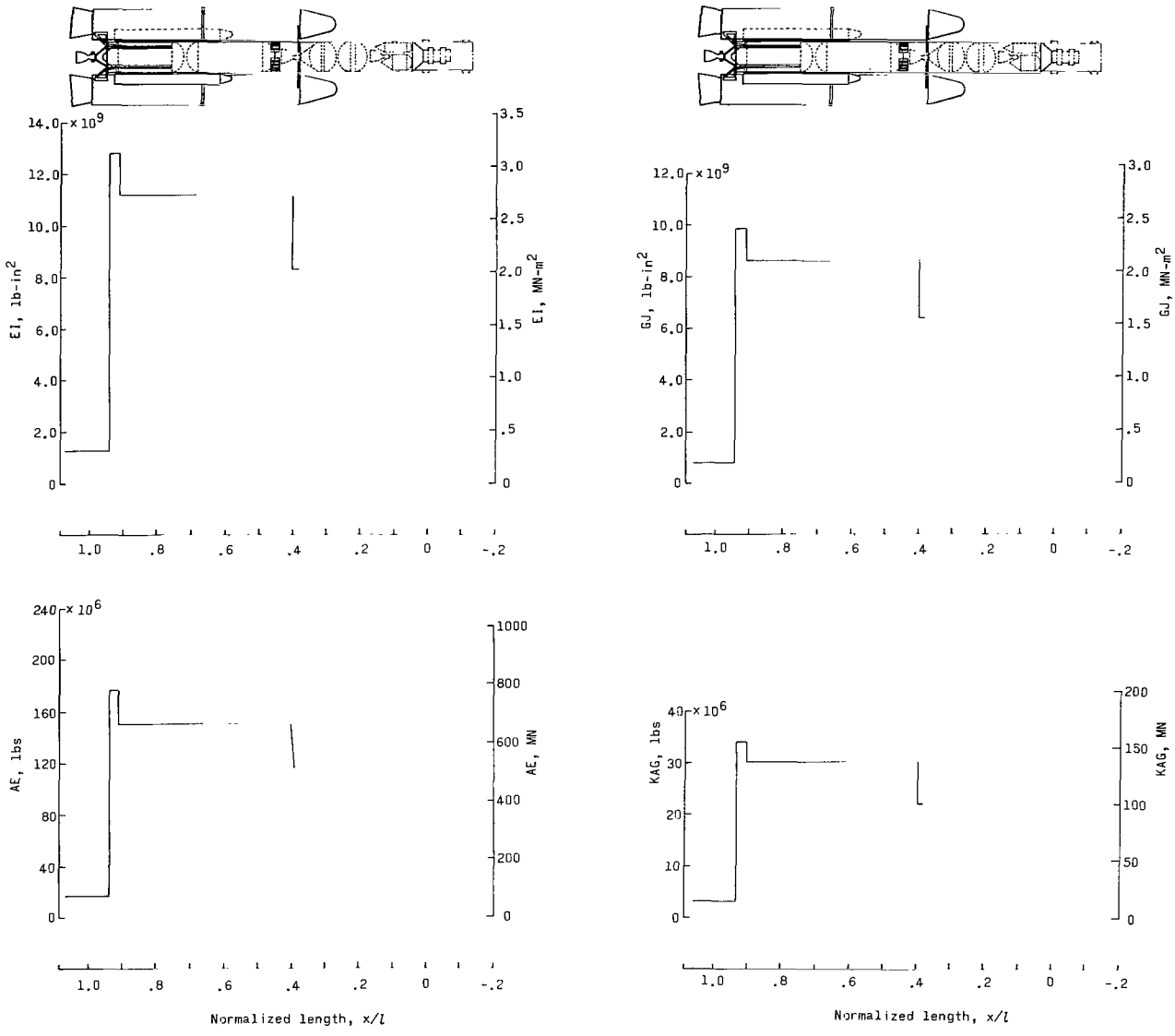

(b) Solid rocket motors.

Figure 6.- Concluded.

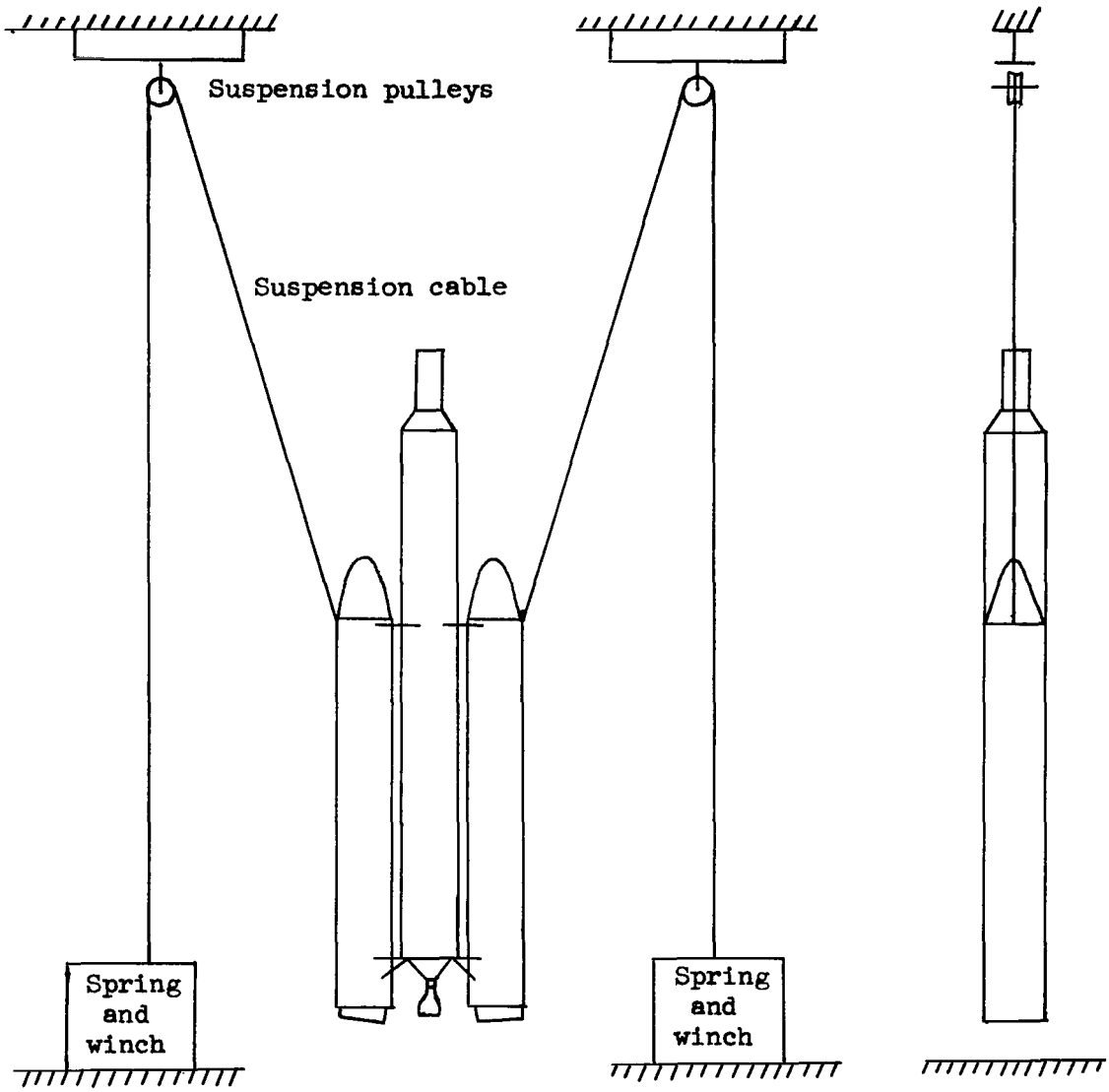

Figure 7.- Schematic of suspension system.

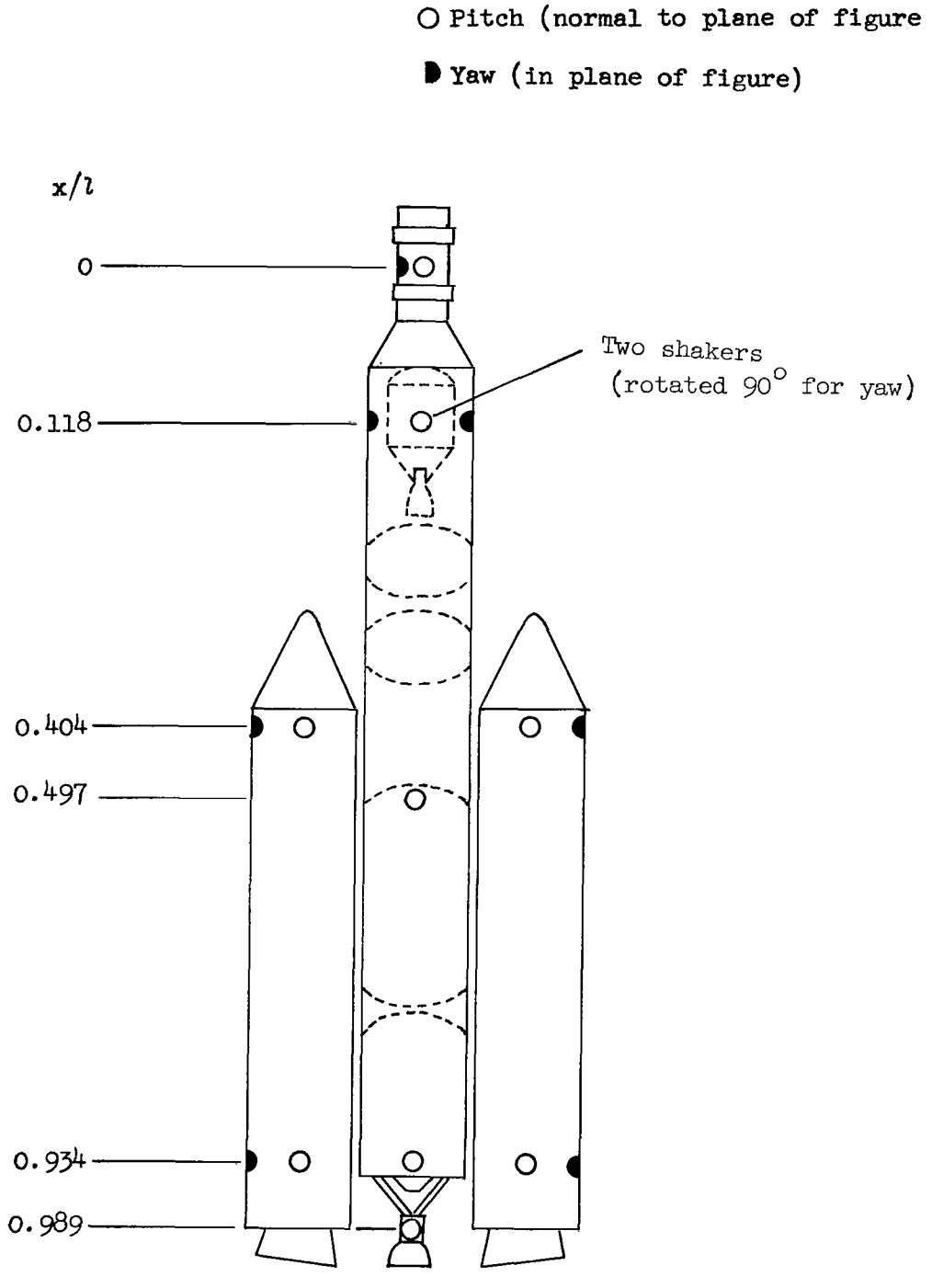

Figure 8.- Location of shakers for all configurations.

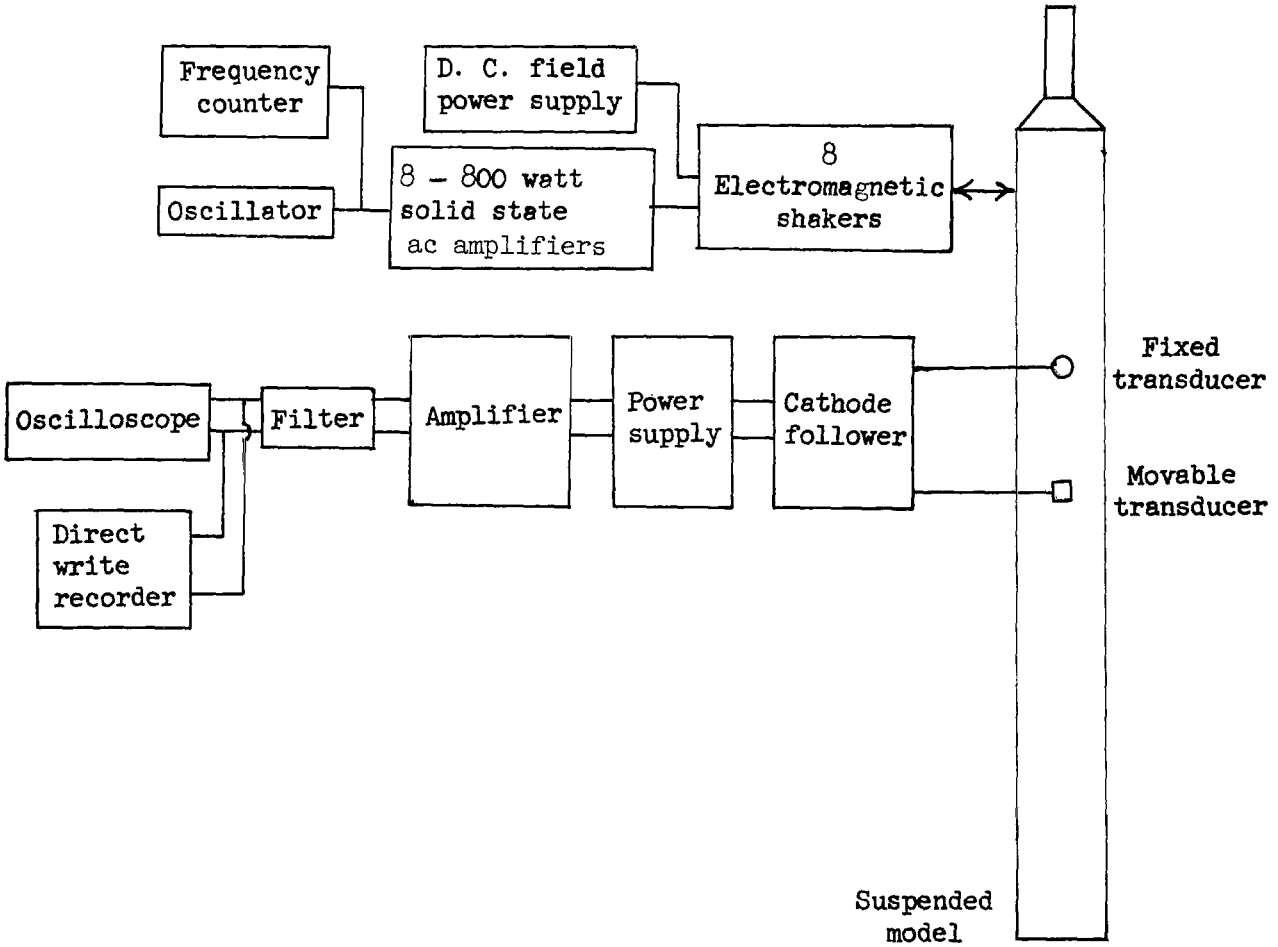

Figure 9.- Schematic of instrumentation system.

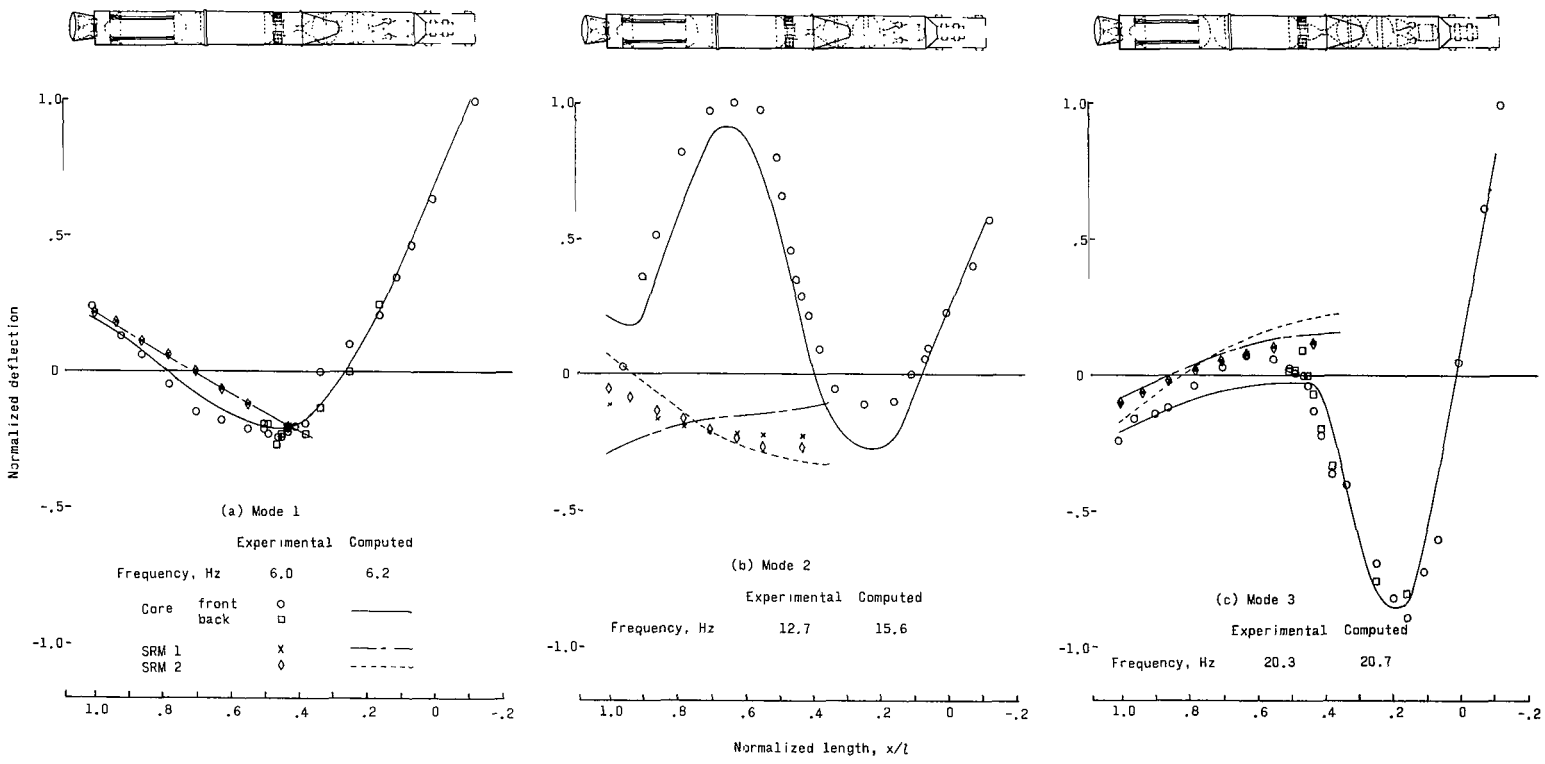

Figure 10.- Comparison of experimental and computed lateral pitch response using the unmodified outrigger flexibility data. t = 0; 26 000 lb (11 790 kg) payload.

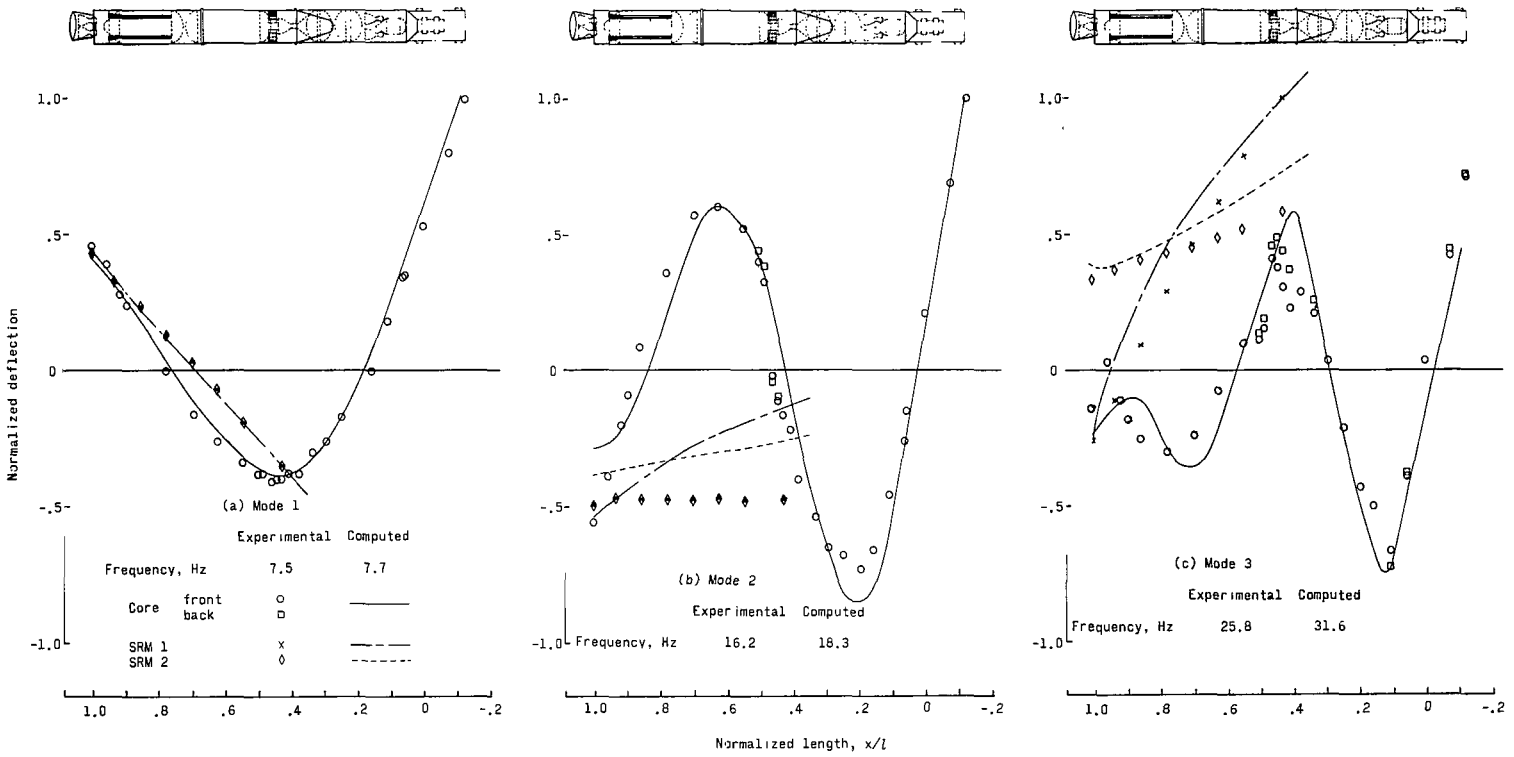

Figure 11.- Comparison of experimental and computed lateral pitch response using unmodified aft outrigger flexibility data. t = 105 seconds; 26 000 lb (11 790 kg) payload.

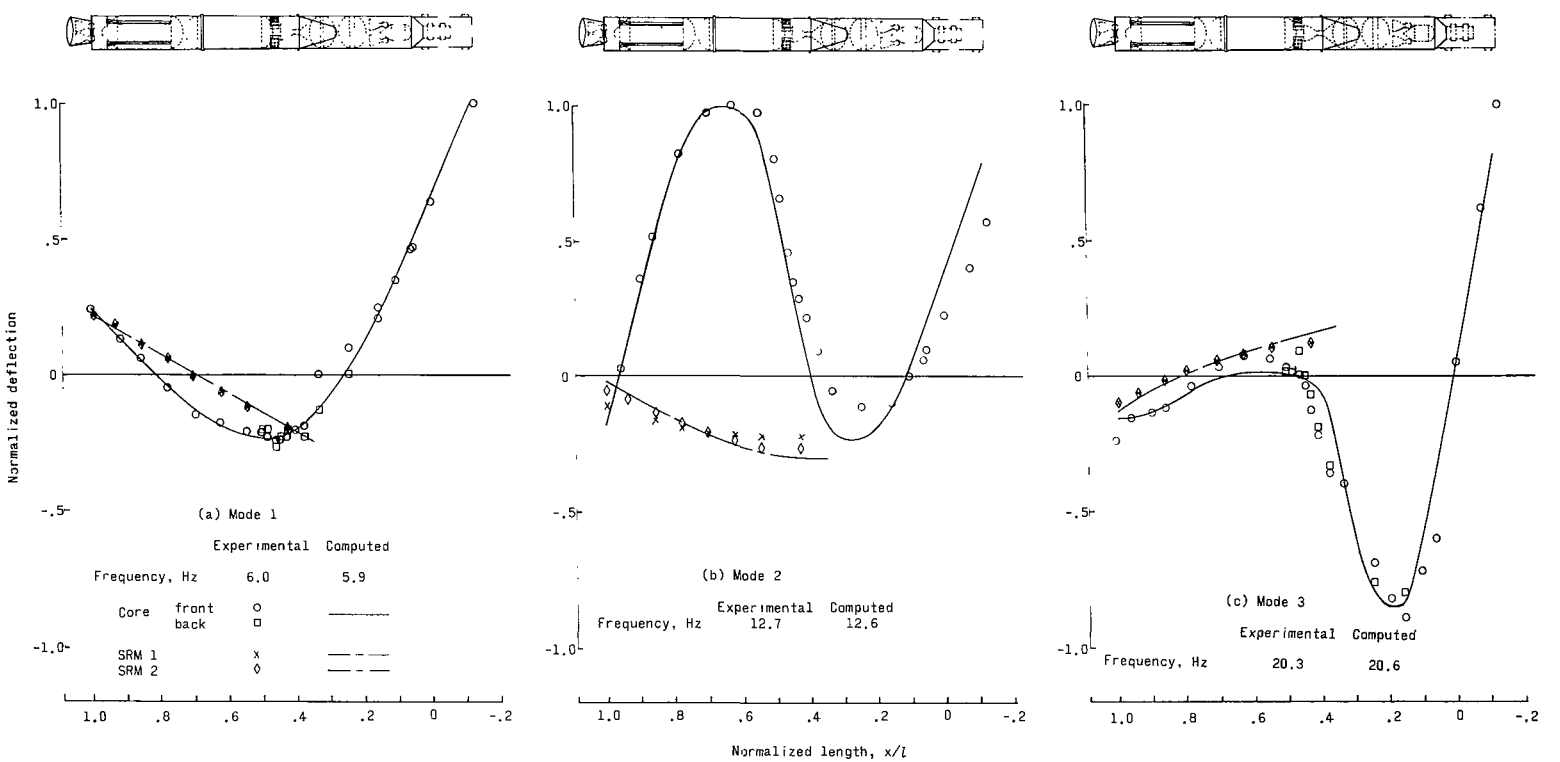

Figure 12.- Measured and computed lateral pitch response using the modified aft outrigger flexibility data. t = 0; 26 000 lb (11 790 kg) payload.

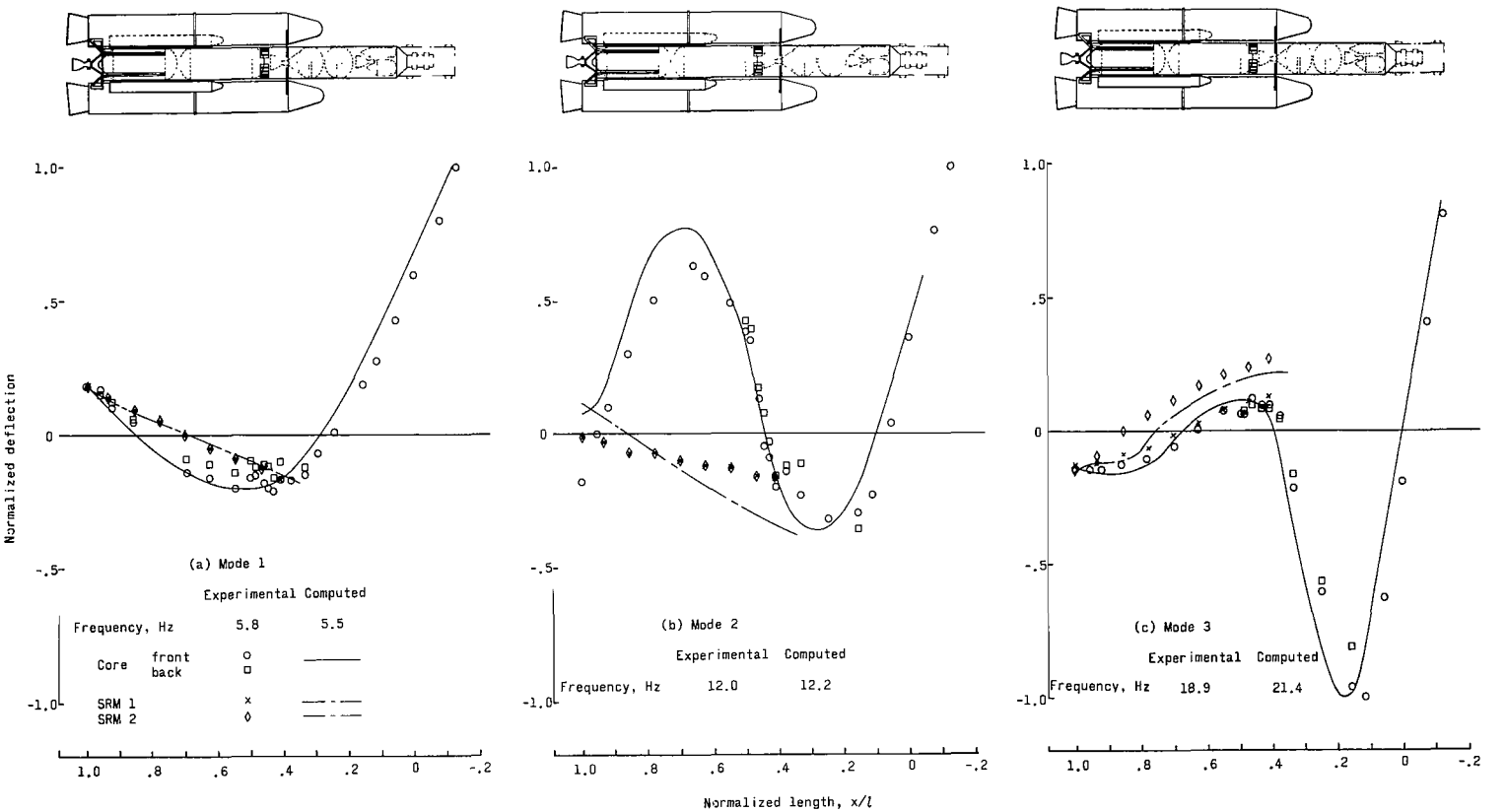

Figure 13.- Measured and computed lateral yaw response using the modified aft outrigger flexibility data. t = 0; 26 000 lb (11 790 kg) payload.

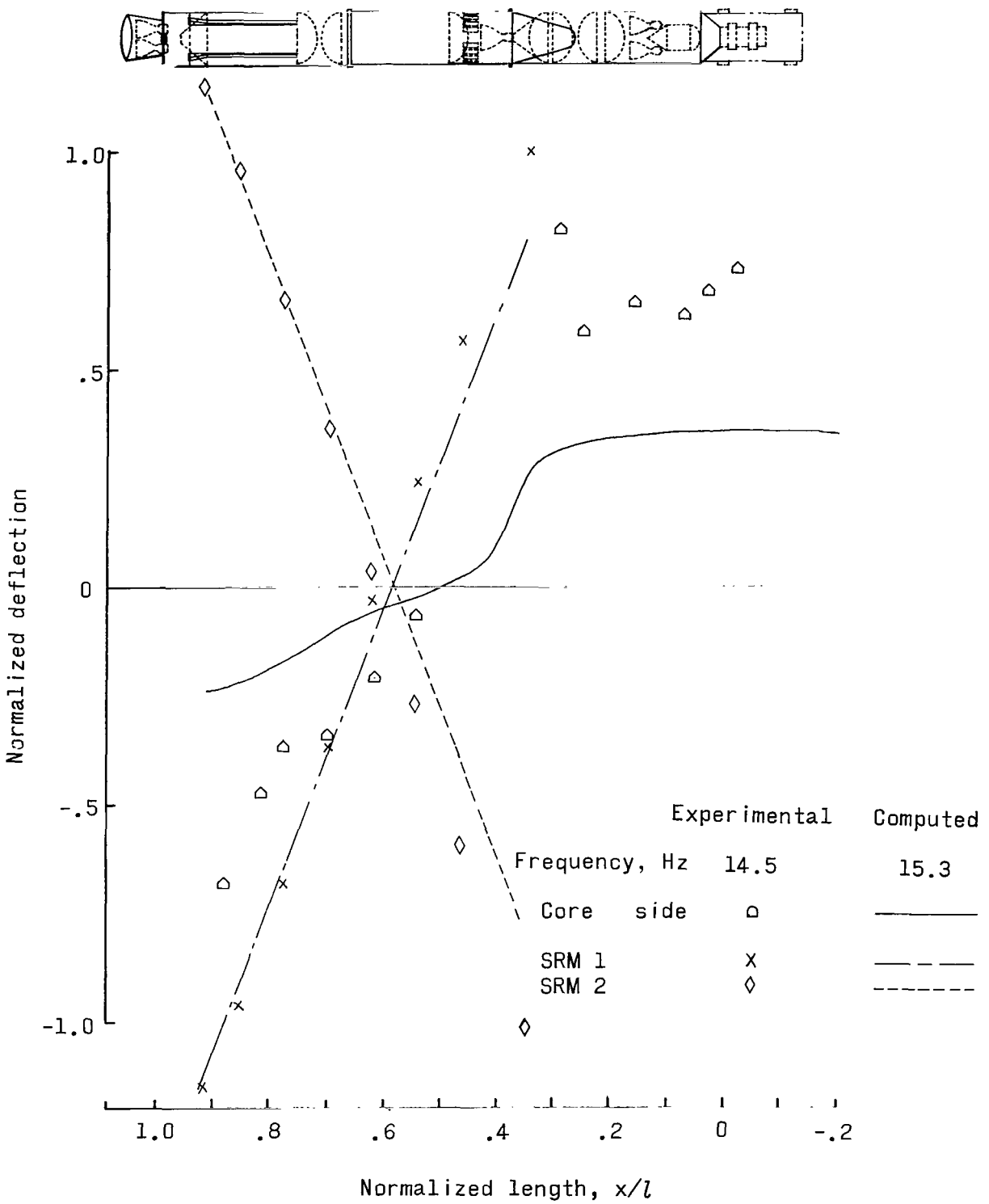

Figure 14.- Measured and computed solid rocket motor asymmetric pitch response using the modified aft outrigger flexibility data. t = 0; 26 000 lb (11 790 kg) payload.

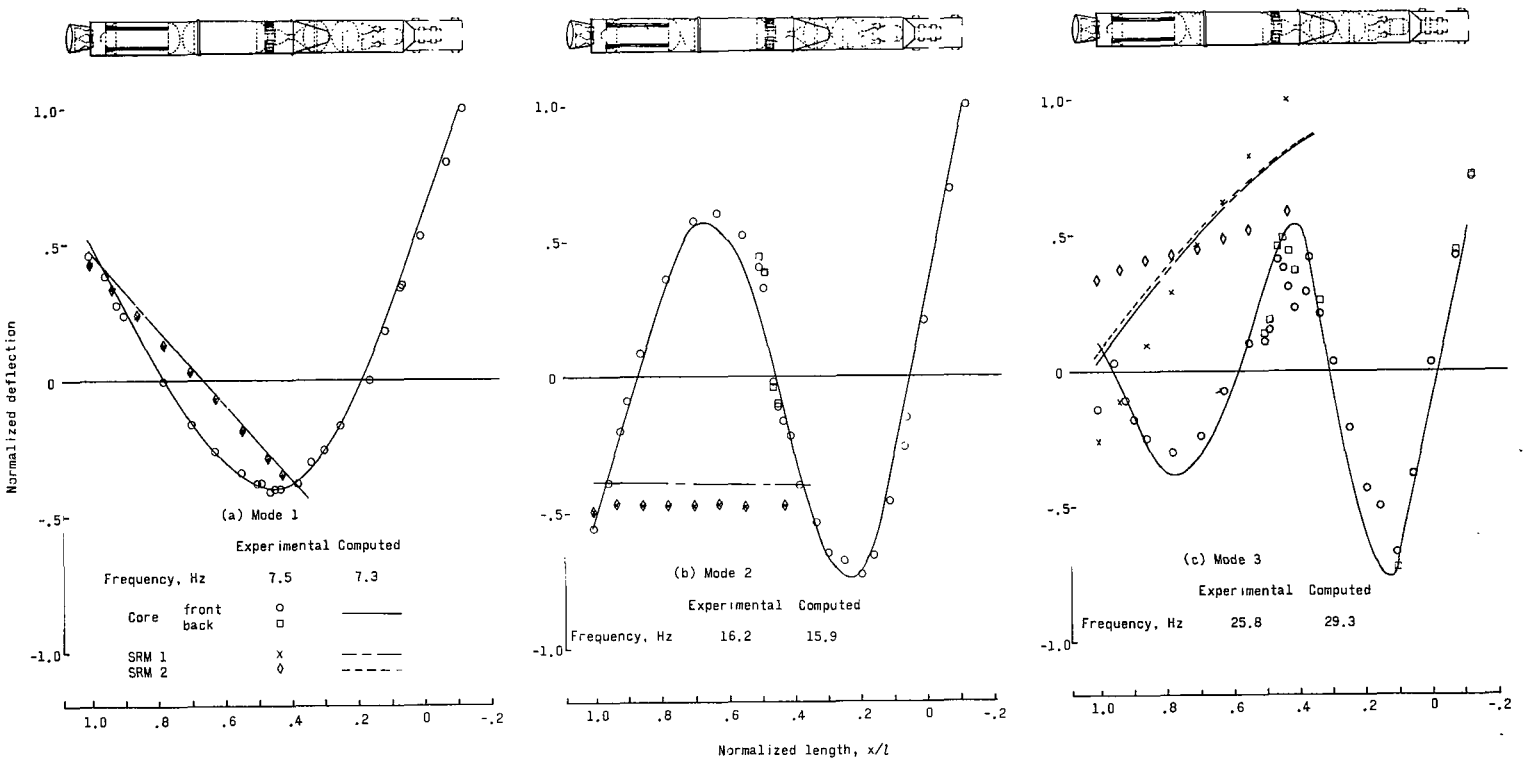

Figure 15.- Measured and computed lateral pitch response using the modified aft outrigger flexibility data.
t = 105 seconds; 26 000 lb (11 790 kg) payload.

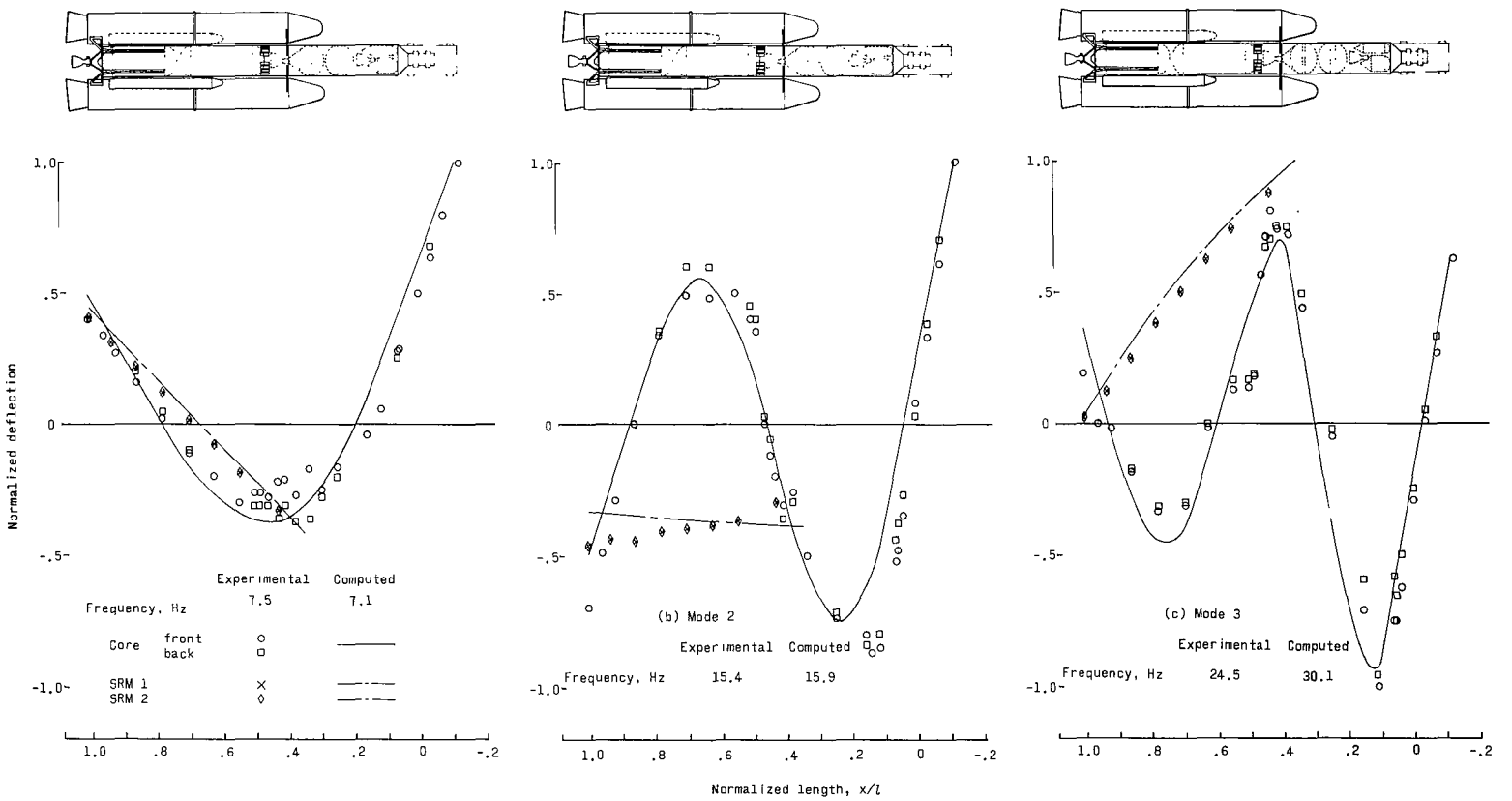

Figure 16.- Measured and computed lateral yaw response using the modified aft outrigger flexibility data. t = 105 seconds; 26 000 lb (11 790 kg) payload.

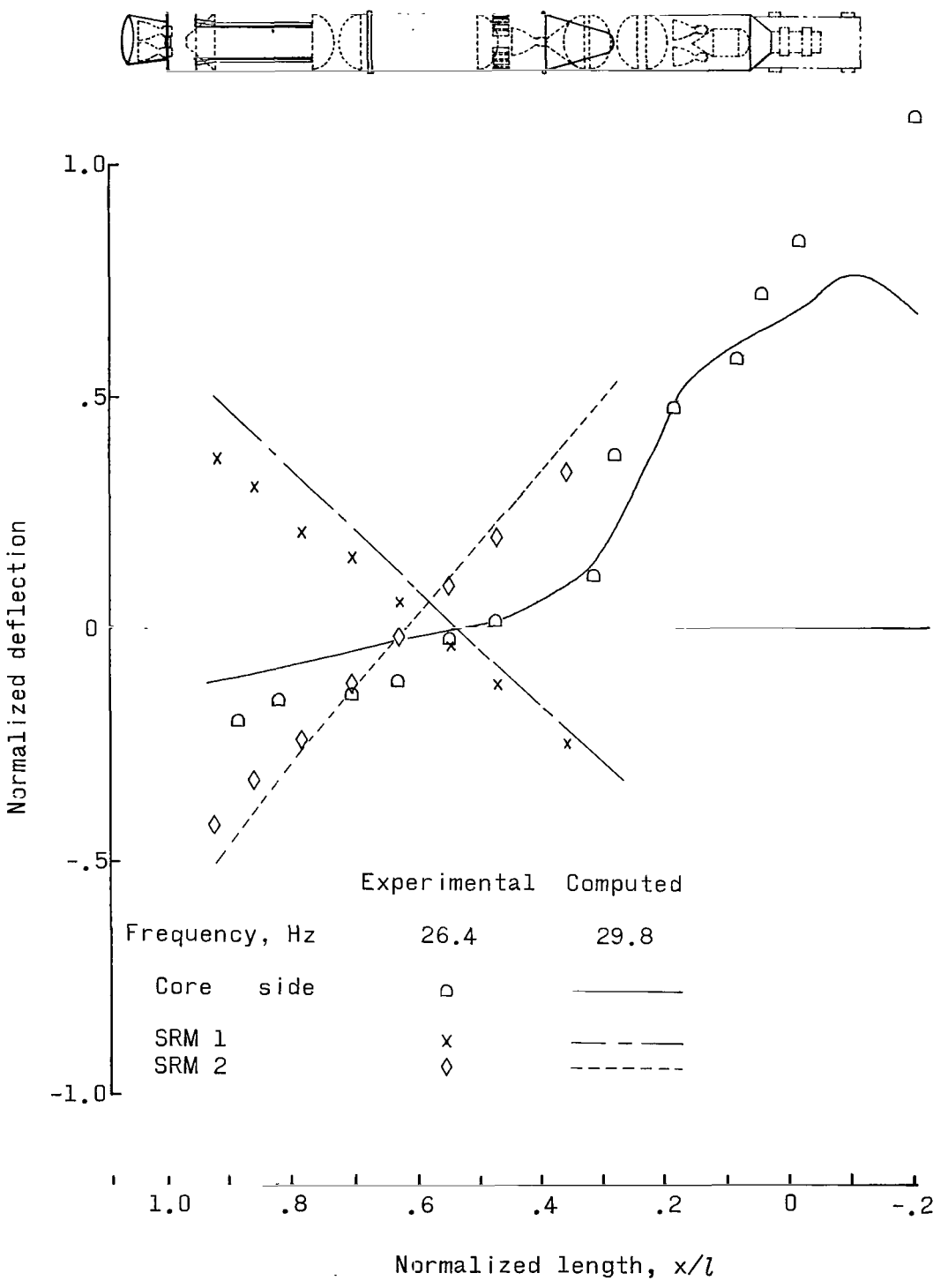

Figure 17.- Measured and computed solid rocket motor asymmetric pitch response using the modified aft outrigger flexibility data. t = 105 seconds; 26 000 lb (11 790 kg) payload.

NATIONAL AERONAUTICS AND SPACE ADMINISTRATION
WASHINGTON, D. C. 20546
OFFICIAL BUSINESS

FIRST CLASS MAIL

POSTAGE AND FEES PAID
NATIONAL AERONAUTICS AND
SPACE ADMINISTRATION

080 001 57 51 3DS 68226 00903
AIR FORCE WEAPONS LABORATORY/AFWL/
KIRTLAND AIR FORCE BASE, NEW MEXICO 87117

ATT I. LOU BOWMAN, ACTING CHIEF TECH. LIB

POSTMASTER: If Undeliverable (Section 158 Postal Manual) Do Not Return

"The aeronautical and space activities of the United States shall be conducted so as to contribute . . . to the expansion of human knowledge of phenomena in the atmosphere and space. The Administration shall provide for the widest practicable and appropriate dissemination of information concerning its activities and the results thereof."

—NATIONAL AERONAUTICS AND SPACE ACT OF 1958

NASA SCIENTIFIC AND TECHNICAL PUBLICATIONS

TECHNICAL REPORTS: Scientific and technical information considered important, complete, and a lasting contribution to existing knowledge.

TECHNICAL NOTES: Information less broad in scope but nevertheless of importance as a contribution to existing knowledge.

TECHNICAL MEMORANDUMS: Information receiving limited distribution because of preliminary data, security classification, or other reasons.

CONTRACTOR REPORTS: Scientific and technical information generated under a NASA contract or grant and considered an important contribution to existing knowledge.

TECHNICAL TRANSLATIONS: Information published in a foreign language considered to merit NASA distribution in English.

SPECIAL PUBLICATIONS: Information derived from or of value to NASA activities. Publications include conference proceedings, monographs, data compilations, handbooks, sourcebooks, and special bibliographies.

TECHNOLOGY UTILIZATION PUBLICATIONS: Information on technology used by NASA that may be of particular interest in commercial and other non-aerospace applications. Publications include Tech Briefs, Technology Utilization Reports and Notes, and Technology Surveys.

Details on the availability of these publications may be obtained from:

SCIENTIFIC AND TECHNICAL INFORMATION DIVISION

NATIONAL AERONAUTICS AND SPACE ADMINISTRATION

Washington, D.C. 20546